RECORD 2020/14

THE UTILITY OF THE METAMORPHIC ROCK RECORD: CONSTRAINING THE PRESSURE–TEMPERATURE–TIME CONDITIONS OF METAMORPHISM

by
FJ Korhonen, DE Kelsey, IOH Fielding and SS Romano

Curtin University
John de Laeter Centre
The University of Western Australia
Achieving International Excellence
Government of Western Australia
Department of Mines, Industry Regulation and Safety
Geological Survey of Western Australia

Government of **Western Australia**
Department of **Mines, Industry Regulation and Safety**

RECORD 2020/14

THE UTILITY OF THE METAMORPHIC ROCK RECORD: CONSTRAINING THE PRESSURE–TEMPERATURE–TIME CONDITIONS OF METAMORPHISM

by
FJ Korhonen, DE Kelsey, IOH Fielding and SS Romano

PERTH 2020

Geological Survey of Western Australia

MINISTER FOR MINES AND PETROLEUM
Hon Bill Johnston MLA

DIRECTOR GENERAL, DEPARTMENT OF MINES, INDUSTRY REGULATION AND SAFETY
David Smith

EXECUTIVE DIRECTOR, GEOLOGICAL SURVEY AND RESOURCE STRATEGY
Jeff Haworth

REFERENCE
The recommended reference for this publication is:
Korhonen, FJ, Kelsey, DE, Fielding IOH and Romano, SS 2020, The utility of the metamorphic rock record: constraining the pressure–temperature–time conditions of metamorphism: Geological Survey of Western Australia, Record 2020/14, 24p.

ISBN 978-1-74168-908-2
ISSN 2204-4345

Isotope and element analyses are routinely conducted using the GeoHistory laser ablation ICP-MS and Sensitive High-Resolution Ion Microprobe (SHRIMP) ion microprobe facilities at the John de Laeter Centre (JdLC), Curtin University, with the financial support of the Australian Research Council and AuScope National Collaborative Research Infrastructure Strategy (NCRIS). The TESCAN Integrated Mineral Analyser (TIMA) instrument was funded by a grant from the Australian Research Council (LE140100150) and is operated by the JdLC with the support of the Geological Survey of Western Australia, The University of Western Australia (UWA) and Murdoch University. Mineral analyses are routinely obtained using the electron probe microanalyser (EPMA) facilities at the Centre for Microscopy, Characterisation and Analysis at UWA, and at Adelaide Microscopy, University of Adelaide.

Published 2020 by the Geological Survey of Western Australia
This Record is published in digital format (PDF) and is available online at <www.dmirs.wa.gov.au/GSWApublications>.

Further details of geoscience products are available from:
Information Centre
Department of Mines, Industry Regulation and Safety
100 Plain Street
EAST PERTH WESTERN AUSTRALIA 6004
Telephone: +61 8 9222 3459 Email: publications@dmirs.wa.gov.au
www.dmirs.wa.gov.au/GSWApublications

Cover image: Packing up the campsite in a claypan about 5 km south of Minilya in the southern Pilbara (photo by Olga Blay, DMIRS)

Contents

Figures

Appendices

The utility of the metamorphic rock record: constraining the pressure–temperature–time conditions of metamorphism

by

FJ Korhonen, DE Kelsey, IOH Fielding and SS Romano

Abstract

Geological processes have shaped the Earth throughout its 4.54-billion-year history. Evidence of changes to pressure (*P*) and temperature (*T*) in the Earth's crust and upper mantle during geological events can be recorded by the mineralogy and textures preserved in metamorphic rocks exhumed to the surface. The development of improved thermobarometric techniques, such as phase equilibria modelling and the use of internally consistent thermodynamic datasets, have enhanced our ability to retrieve more precise and reliable *P–T* data from metamorphic rocks. These data can also be integrated with age, chemical and textural information from datable accessory minerals to better define *P–T*–time (*t*) paths. The apparent thermal gradients calculated from *P–T* data relate directly to the thermal regime at the time of metamorphism, which can be used to infer geodynamic setting and heat source, whereas the overall shape of the *P–T–t* path reflects the relative rates of burial and heating vs cooling and exhumation. Together these data can be used to define a sequence of geological events and to identify tectonothermal drivers. This contribution aims to provide geoscientists, and those with an interest in Earth evolution, with a brief overview of both the scientific rationale and methodology used by the Geological Survey of Western Australia in constraining *P–T–t* paths from metamorphic rocks, and the utility of these data.

KEYWORDS: metamorphic evolution, metamorphism, mineral chemistry, monazite, phase diagrams, phase equilibria, thermal gradients

Introduction

The geology of Western Australia spans 4.4 billion years of Earth's history. This history is preserved in the rock record, and we are using a multidisciplinary approach in order to better define the geological framework of Western Australia and its mineral resources. Most exposed rocks in Western Australia have been subjected to changes during their long histories. Metamorphism is the change that occurs in rocks due to variations in pressure (*P*), temperature (*T*) or chemically active fluids resulting from geological events. These changes directly express the evolving thermal regime of the crust and/or lithosphere, which in turn reflects the geodynamics driving the metamorphism. Variations in *P*, *T* and fluids change the mineralogy of rocks, as well as the compositions of the minerals. Consequently, the mineral assemblages preserved in a metamorphic rock provide a record of the *P–T* conditions during an event. Further, the sequence of mineral growth provides a record of the changes in *P* and *T* to which the rock mass was subjected, and provides valuable information for deciphering the underlying tectonic and geodynamic processes that drove the metamorphism. Our ability to interpret the evidence recorded by metamorphic rocks is critical to understanding their history and to constraining terrane evolution models.

Evidence for the metamorphic evolution of a terrane will be recorded on a variety of scales by a variety of different signatures. A major challenge in these studies is to unravel a composite history. Thermobarometry is the science of quantifying the *P–T* conditions at which a mineral assemblage developed. However, metamorphism is a dynamic process, involving changes in these variables through time. The *P–T*–time (*t*) path of a metamorphic rock is the set of all *P–T* conditions experienced by a rock during its metamorphic history. An important goal in any metamorphic study is the reconstruction of the *P–T–t* path, although resolving the *P–T–t* history for all stages of metamorphic evolution is challenging. Over the last few decades, methods have been refined to resolve the depth, thermal, temporal, deformation and mineralization history of geological terranes. Detailed observations from map- to thin-section scale can now be integrated with element and isotope data and phase equilibria modelling to retrieve more precise and reliable *P–T–t* data from rock samples. An integrated approach using these modern methods of metamorphic petrology is now routinely being applied by the Geological Survey of Western Australia (GSWA) to enhance our understanding of the tectonometamorphic evolution of Western Australia. This Record specifically discusses some of the techniques that are currently being used to improve data coverage, and some of the assumptions and limitations associated with these methods.

Workflow applied to metamorphic studies

This Record describes the workflow with relevant background and analytical details for Metamorphic History Records released by GSWA. A summary of the workflow is provided in Appendix 1. Seminal references or published examples illustrating some of the scientific concepts are listed in Appendix 2. Abbreviations for common metamorphic phases are defined in Appendix 3. Most thermobarometric estimates are based on the results of phase equilibria forward modelling. For some samples, mineral chemistry may also be integrated with phase equilibria modelling or used for conventional thermobarometry. Methodological details for thermobarometric estimates based on methods other than phase equilibria modelling are provided within the individual Metamorphic History Records for those samples. Many of the samples are also dated using in situ geochronology, whereby the datable mineral is analysed in thin section to retain its microstructural context, as this can be invaluable information in terms of interpreting the age significance. The geochronological data and a brief interpretation are provided in an accompanying Geochronology Record, which is referred to in the Metamorphic History Record, as appropriate. Each Metamorphic History Record describes the sample analysed, the results and a brief interpretation. The broader geological implications of the data may be published elsewhere. Some Records describe results for samples analysed by collaborators external to GSWA, in which case additional analytical information not documented here may be included within the individual Records. Release of new Metamorphic History Records occurs throughout the year as they are completed.

Sample collection and field observations

Most samples have been assigned to tectonic and lithostratigraphic units based on the interpretation of field relationships and any geochronological results at the time of publication. These assignments, and the currency of lithostratigraphic and tectonic units, may subsequently be revised, and up-to-date information should be obtained from the latest GSWA publications. Field observations collected at the outcrop are considered in the interpretation of the *P–T–t* results and relevant relationships may be presented in the Metamorphic History Record. Sample location grid references in Metamorphic History Records refer to the Geocentric Datum of Australia 2020 (GDA2020)*. Locality coordinates for the majority of samples were obtained using a handheld Global Positioning System (GPS) receiver, are accurate to better than ±100 m, and are referenced using Map Grid Australia (MGA) coordinates.

Petrography

The minerals preserved in a rock sample and their textural relationships provide a record of the evolving metamorphic conditions. Thus, any metamorphic study relies on an interpretation of the coexisting minerals — the so-called mineral assemblage — that may have been stable at different times throughout the evolution and, if possible, identification of any mineral reactions that resulted in changes to the mineral assemblage with time. Petrographic observations are made using standard optical microscopy, in addition to analytical scanning electron microscopy (SEM), as appropriate. Thin sections are mapped with the Tescan Integrated Mineral Analyser (TIMA) in the John de Laeter Centre at Curtin University, which is an SEM equipped with four fully integrated energy dispersive spectroscopy (EDS) detectors. This system can identify minerals in situ, characterize the spatial distributions of minerals, and quantify abundances (Fig. 1). More detailed mineral characterization may be conducted using conventional SEM to resolve small-scale features that are difficult to see with an optical microscope or to confirm mineral identification. For some phases, such as the aluminosilicate polymorphs, Raman spectroscopy may be used for mineral identification. Mineral abbreviations adopted by GSWA are defined in Appendix 3, modified from Whitney and Evans (2010).

In situ geochronology and petrochronology

A major goal in modern metamorphic studies is to constrain the absolute timing and duration of metamorphic events and to link these ages to the overall *P–T* evolution. Many minerals can be dated using isotopic techniques, and the U–Th–Pb system is used commonly for determining the ages of geological materials. Zircon, monazite, baddeleyite, xenotime, titanite, apatite and rutile are minerals that incorporate U and/or Th and can be dated using U–Th–Pb geochronology, although their individual suitability for dating metamorphic events varies. The primary minerals GSWA uses to date metamorphism are zircon and monazite, although other minerals may be used on a case-by-case basis. Zircon can dissolve and reprecipitate during metamorphism, particularly under high-temperature conditions and partial melting, forming new grains or overgrowths on pre-existing grains. However, zircon is typically less useful for constraining the age of metamorphism in rocks that have not partially melted, in which case other minerals are better geochronology targets. Monazite is generally more susceptible to dissolution and regrowth than zircon and thus can be more useful for evaluating the history of fluid flow and metamorphism over a wider range of *P–T* conditions. Other minerals listed above are not as widely used for geochronology, because they are less common in rocks, or the presence of common Pb can compromise data quality, or the closure temperature for Pb diffusion in such minerals is lower than it is in zircon and monazite.

* GSWA compliance with GDA2020 is estimated to occur mid-2021. Please refer to the information within individual products for up-to-date datum information

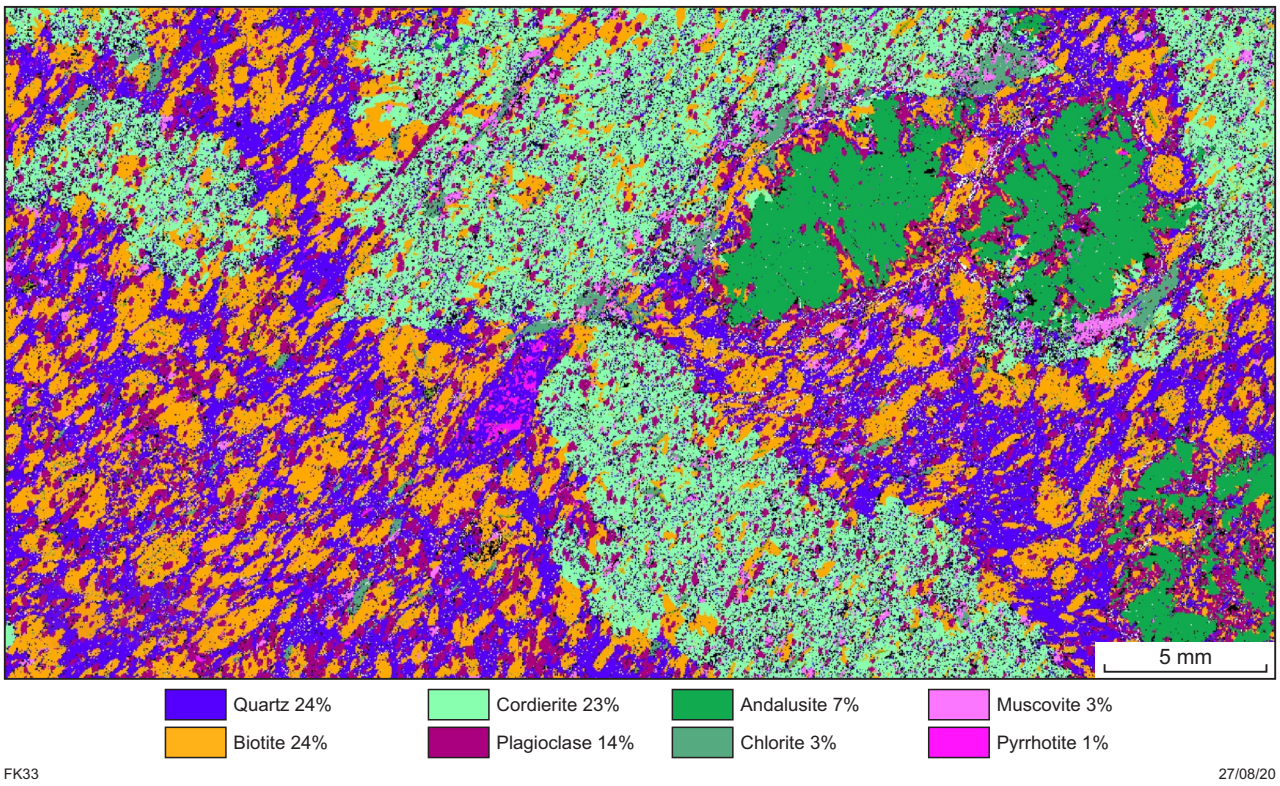

Figure 1. Full thin section TIMA image of a pelitic schist sample with mineral abundances ('modes') calculated within the TIMA software

Accessory minerals that can be targeted for geochronology are generally stable over a large range of metamorphic *P–T* conditions. Therefore, linking the timing of accessory mineral growth with the growth of major rock-forming silicate minerals is essential for resolving the *P–T–t* history. Petrochronology is a relatively new branch of earth science that uses chemistry, textures and phase equilibria modelling to integrate ages with the interpreted reaction sequences of major minerals. Garnet, plagioclase and zircon are the main minerals used in petrochronology because of the distinctive behavior of trace elements in and between these minerals. Rare earth element (REE) minerals such as monazite, xenotime, allanite and apatite are also playing an increasingly important role in petrochronology. Garnet is an important reservoir for heavy rare earth elements (HREE) and Y, whereas plagioclase strongly partitions Eu and Sr over the other major rock-forming minerals. Zircon and monazite are also a sink and source of these elements, and exchange these elements with the major rock-forming minerals. Thus, the growth and consumption of these minerals can be tracked via the chemistry of accessory minerals, such that relative enrichment or depletion in these elements may reflect the consumption or growth of major minerals. For example, accessory minerals growing in equilibrium with garnet tend to be relatively depleted in HREE, as these elements would preferably partition into garnet (Fig. 2).

A recent advance in metamorphic studies at GSWA is the routine in situ analysis of monazite for geochronology. Monazite crystals are first identified in polished thin sections from the TIMA images, and then imaged in detail using high-contrast backscattered electron (BSE) methods, to reveal internal structure and compositional zoning (Fig. 3a). Monazite crystals are selected for analysis based on their size (>10 μm), suitability (e.g. absence of cracks, mineral inclusions, alteration), petrographic (textural) setting and internal zoning patterns. Multiple analyses on individual crystals target different zones to test for potential age differences, whereas areas containing cracks and inclusions are avoided. Monazite grains are analysed in 25 x 48 mm polished thin sections, so that textural relationships between the dated minerals and major rock-forming minerals are preserved. Quantitative U–Th–Pb age data are typically obtained with laser ablation inductively coupled plasma mass spectrometry (LA-ICP-MS), although the Sensitive High-Resolution Ion Microprobe (SHRIMP) may be used for some samples, that is, those with monazite that are particularly low in U. For selected samples, REE chemistry of monazite grains may be acquired simultaneously using laser ablation split stream (LASS) methods or separately using a quadrupole ICP-MS or an electron probe microanalyser (EPMA). For some individual grains, high-resolution X-ray maps of Th, U, Pb and Y (Fig. 3b–e) can be used to calculate age maps (Fig. 3f). Although the age uncertainties are significant (typically >100 Ma), these maps can reveal the spatial distribution of ages in a single grain or differentiate between growth events that are widely spaced in time (Fig. 3f). Analytical details for U–Th–Pb geochronology and any trace element data collected by ICP-MS are provided in the Introduction to Geochronology Information document released each year on the accompanying data package (e.g. Lu et al., 2020).

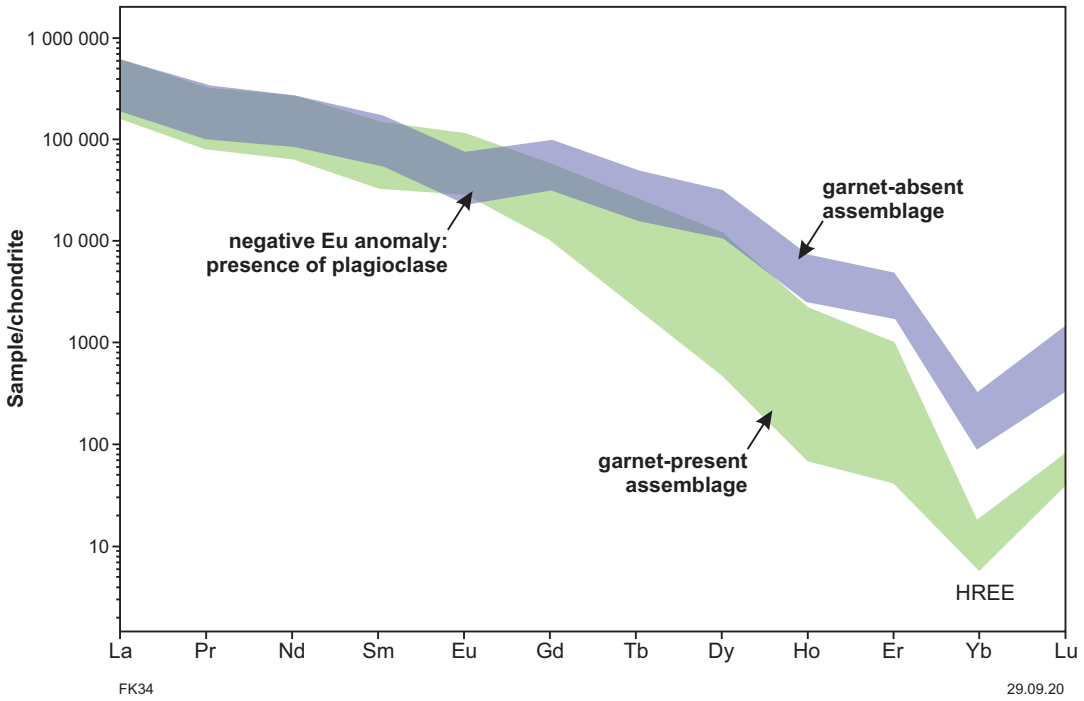

Figure 2. **Examples of chondrite-normalized trace element data for monazite. Blue shading shows range of monazite analyses from a garnet-absent assemblage; green shading shows range of analyses from a garnet-bearing assemblage. HREE will preferentially partition into garnet over monazite, so monazite that crystallizes in equilibrium with garnet generally has lower HREE concentrations compared to monazite that grew without garnet. The negative Eu anomaly (blue data) is also consistent with monazite growth in the presence of plagioclase. This example shows plots from two different assemblages, but a similar relationship could be observed in a single sample: monazite growing in equilibrium with garnet (e.g. prograde monazite and garnet) will have lower HREE, whereas monazite growing during garnet breakdown (e.g. retrograde monazite) will have elevated HREE as these elements are liberated from garnet**

Mineral chemistry

Mineral compositions (and mineral modal abundance) will change as a function of *P* and *T* as minerals grow or are consumed. Consequently, mineral compositions and textures can record the conditions at which a rock equilibrated, and in some cases, they may offer insight into the evolving *P–T* path.

Analytical details for routine mineral chemistry

Mineral chemistry data are acquired using an EPMA. Most EPMAs can analyse a broad range of elements (typically F–U), although operating conditions will vary as a function of characteristic X-ray energy intrinsic to the element and the concentration of that element in the material. Types of mineral chemistry data include quantitative point data and elemental mapping.

Quantitative point data

Unless otherwise reported, point data are measured using a Cameca SXFive equipped with five wavelength-dispersive spectrometers (WDS) at Adelaide Microscopy, The University of Adelaide. For standard major element analyses in silicate minerals, instrument operating conditions include an accelerating voltage of 15 kV and a beam current of 20 nA. The standard list of elements analysed for most minerals includes Fe, Mg, Mn, Ca, Si, Al, Na, K, Ti, Cr, Zn, Cl and F, although this list can be changed as required. A focused beam is normally used, although some phases containing Na, such as feldspar, may require a defocused beam. Calibration is performed on certified natural and synthetic standards from Astimex Ltd. and P&H Associates. Mean atomic number (MAN) background correction is used, and data are calibrated and reduced using Probe for EPMA, distributed by Probe Software Inc. Quantitative point data for minor and trace element chemistry may require different operating conditions.

Quantitative element maps

High-resolution WDS quantitative element maps for selected phases or domains are obtained with a JEOL 8530F Hyperprobe at the Centre for Microscopy, Characterisation and Analysis, The University of Western Australia, unless otherwise reported. Normal operating conditions include a 40° take-off angle, an accelerating voltage of 15 kV, and a variable beam current (80–250 nA), depending on the analysis. The beam is typically fully focused. Dwell time per pixel and pixel dimension will vary and are adjusted for the map size. On-peak counting times are 20 s. The standard element list for most maps

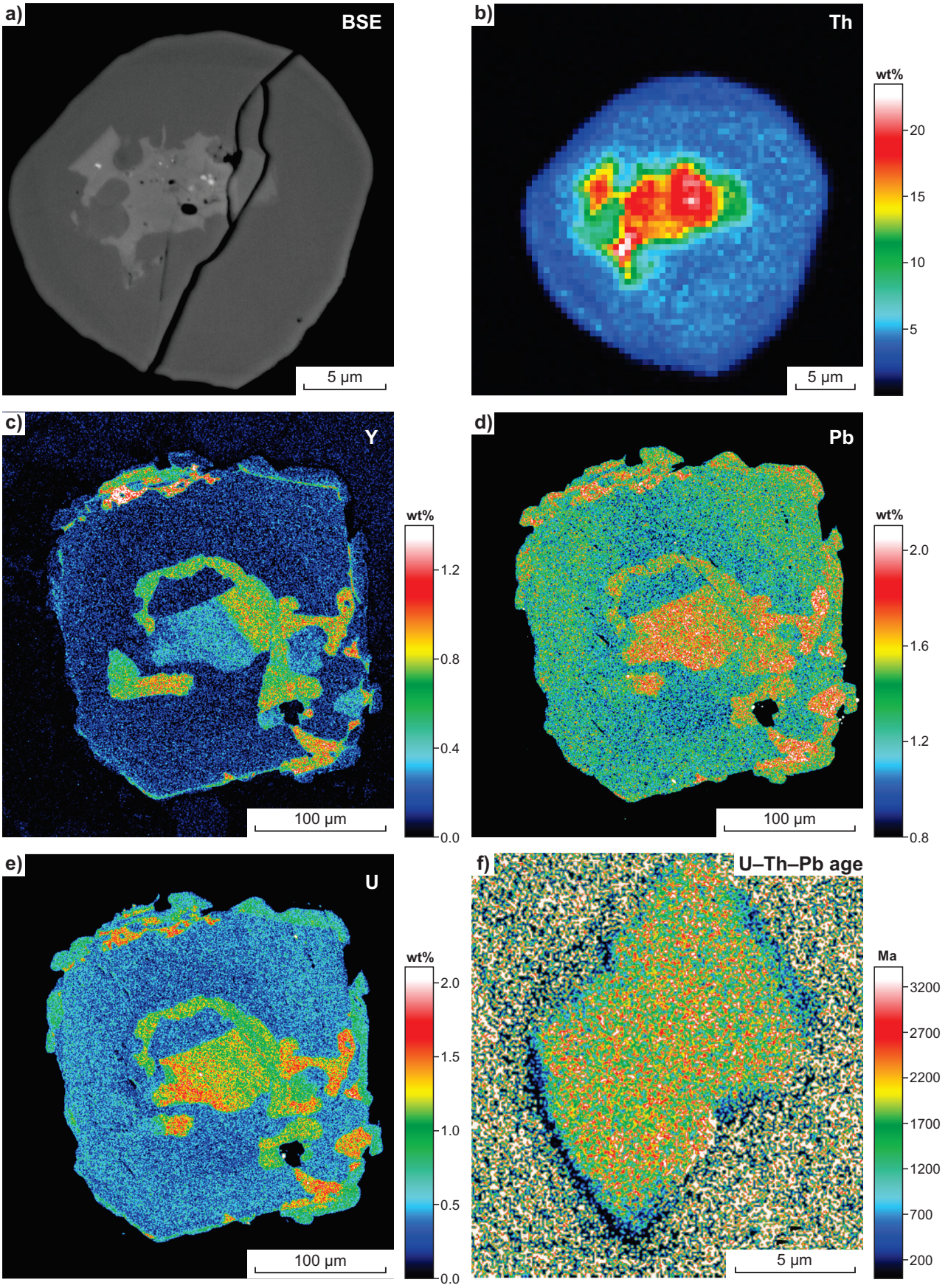

Figure 3. **Examples of images characterizing monazite used for in situ geochronology and petrochronology: a) BSE image; b) quantitative element map of Th from (a); c) Y element map; d) Pb element map from (c); e) U element map from (c); f) monazite age map calculated using Th, U, Pb and Y concentrations. In this example, the Paleoproterozoic monazite has a very thin 500 Ma rim (dark blue) that corresponds to known geological events in the region. BSE image collected with SEM; elemental and age map acquired with EPMA**

includes Fe, Mg, Mn, Ca, Si, Al, Na, K, Ti and Cr, although this list may be subject to change. Element maps for monazite include La, Ce, Pb, Y, Th, P, U and Ca. Matrix corrections of Armstrong/Love-Scott (Armstrong, 1988) and MAN background are applied. Image processing is performed offline with the CalcImage software.

Mineral chemistry data used for thermobarometric estimates are summarized in the Metamorphic History Record. Compositional parameters that define the chemistry of individual minerals are typically reported using THERMOCALC notation (e.g. White et al., 2014a,b); relevant variables are defined in individual Records. Additional analytical information not documented here may be included within individual Records.

Thermobarometry

Thermobarometry is the quantitative determination of the *T* and *P* at which a metamorphic or igneous rock reached chemical equilibrium. The assumption of attainment of thermodynamic equilibrium — at some length scale — between coexisting minerals is a fundamental underlying principle of all types of thermobarometry (e.g. Powell and Holland, 2008). Three types of thermobarometric techniques can be used to quantify these *P–T* conditions, with each technique having various advantages and disadvantages.

Conventional thermobarometry

Conventional thermobarometry aims to quantify the *P–T* conditions of a specific chemical reaction that relates element exchange between end-members of two or more minerals in the preserved mineral assemblage, where an end-member is a fixed pure composition component of a phase. For example, natural garnet shows compositional variation, and thus element exchange, between Fe, Mg and Ca. Therefore, fixed pure composition components that can be used — when mixed in varying proportions — to express the composition of garnet are those for Fe, Mg and Ca end-members, respectively, which for garnet are $Fe_3Al_2Si_3O_{12}$ (almandine), $Mg_3Al_2Si_3O_{12}$ (pyrope) and $Mg_3Al_2Si_3O_{12}$ (grossular). Reactions used as thermometers are mainly *T*-dependent, and define steep slopes on a conventional *P–T* diagram (Fig. 4a). Reactions used as barometers are mainly *P*-dependent and have shallow slopes in *P–T* space (Fig. 4a). The application of a thermometer or barometer requires the composition of the minerals, the thermodynamic data for end-members, and a calibration that relates the mineral chemistry to *P* and *T* (see Spear, 1993 for a review of common conventional thermobarometers).

The intersection of two different reactions in *P–T* space can be used to define a unique *P* and *T* of equilibration (Fig. 4a). The most widely applied thermometers are cation exchange reactions, such as Fe–Mg exchange between two minerals. Over the last decade, thermometers have been developed that use trace element concentrations in minerals, such as Ti-in-quartz, Ti-in-zircon, Zr-in-titanite and Zr-in-rutile. The Y concentration of coexisting monazite and garnet is another trace element thermometer that can be applied to metamorphic rocks. The most common barometers are net transfer reactions that involve the consumption of existing minerals and the growth of new ones. Attempts to calibrate a new barometer using the stored stress in mineral inclusions have recently gained attention. This technique relies on measuring subtle peak shifts using laser Raman microspectrometry, and has most widely been applied to quartz inclusions hosted in garnet.

The advantage of using published thermobarometers is that they are relatively easy to use; they simply require mineral composition data. However, there can be potentially significant sources of uncertainty in conventional thermobarometry. Analytical uncertainties may include the mineral composition analyses, in particular the amount of Fe^{3+} (versus Fe^{2+}), which cannot be measured directly, as well as the thermodynamic data and the calibration method. Propagation of these analytical uncertainties are typically in the order of ±50°C for *T* and ±1 kbar for *P*, although depending on the mineral composition, these uncertainties may be much greater. Another significant source of uncertainty is that (outside the use of internally consistent databases and software such as THERMOCALC, see below) the thermodynamics — and uncertainties — of individual thermometers and barometers are not consistent or correlated with each other as different researchers developed them all independently. This means that it is difficult to assess the validity of results obtained via the intersection of different thermometers and barometers, and to make comparisons of the results. Other potential uncertainties may include determining whether the phases truly represent an equilibrium assemblage, or whether any subsequent modification to their compositions has occurred during later geological events. These limitations are discussed in more detail below.

Multiple-reaction thermobarometry

Multiple-reaction thermobarometry ('optimal thermobarometry' of Powell and Holland, 1994) attempts to minimize some of the analytical uncertainties associated with conventional thermobarometry through the use of an internally consistent dataset of thermodynamic properties (Berman, 1988; Powell and Holland, 1988). With the use of an internally consistent dataset, the calculated *P* and *T* results and uncertainties are all correlated to each other, which means that the result including uncertainty is statistically meaningful. An independent set of end-member reactions is calculated from the compositions of minerals that are inferred to have reached chemical equilibrium (Fig. 4b). The primary software that is used for optimal thermobarometric calculations is 'averagePT' (avPT) in the program THERMOCALC (Powell and Holland, 1988), which uses the internally consistent Holland and Powell (1998, 2011) dataset. In avPT, the thermodynamics of the end-member reactions are combined statistically by a least squares method to give an optimal estimate of *P* and/or *T* (Powell and Holland, 1994; Fig. 4b). The software also calculates an uncertainty, a goodness-of-fit value and other diagnostic parameters, which allow assessment of the degree to which a sample has equilibrated that is not possible with conventional thermobarometry. An additional advantage of this technique over conventional thermobarometry is that all minerals interpreted to be in the equilibrium mineral assemblage can be used in a single (simultaneous) avPT calculation. The most significant disadvantages to this approach are that minerals either may not retain the equilibrium composition due to cooling or

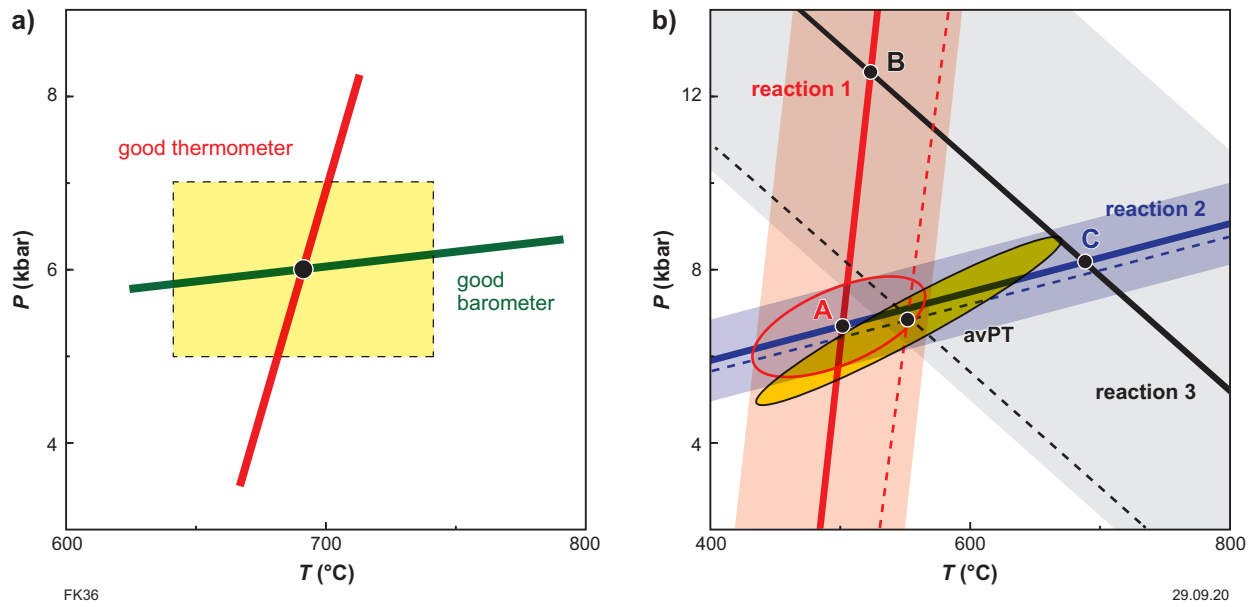

Figure 4. **Schematic representations of thermobarometers: a) *P–T* diagram showing that conventional thermometers have steep slopes and barometers have shallow slopes in *P–T* space. The intersection of these reactions defines the *P–T* conditions of equilibration for the mineral assemblage (small black circle). The typical uncertainties for conventional thermometers (±50°C) and barometers (±1 kbar) are shown by the dashed yellow box; b) multiple-reaction thermobarometry (avPT in THERMOCALC) uses an independent set of reactions calculated from the compositions of minerals inferred to have reached chemical equilibrium. In this example, reactions [1], [2] and [3] (solid lines with uncertainties represented by shading) generate three intersections A, B and C. The optimal *P–T* (filled circle labelled 'avPT') lies within the region where all three uncertainty bands overlap (dashed lines). The correlated uncertainties in reactions [1], [2] and [3] (and hence in A, B and C) cause the optimal *P–T* to lie outside the triangle ABC, and to have a highly flattened uncertainty ellipse (shown in yellow), implying that *P* is well determined if a good estimate of *T* can be made. The red ellipse shows the results based on reactions [1] and [2] alone, for comparison. Modified from Powell and Holland (1994)**

retrogression, resulting in either significant uncertainties or failed calculations, and/or that the compositions of minerals used in the calculations do not actually represent coexisting equilibrium compositions. Interpreting which compositions to use for minerals that preserve compositional zoning also introduces uncertainty, although these discrepancies can be identified and possibly corrected with the diagnostic parameters in the software.

Phase equilibria modelling

Phase diagrams are graphical representations ('maps') of the phases that stably coexist (the stable mineral assemblages) as a function of different thermodynamic variables such as *P* and *T* and/or composition (Fig. 5). These diagrams are calculated using internally consistent datasets of the thermodynamic properties of minerals, fluids and melts in combination with activity–composition (*a–x*) models for these phases (e.g. Powell et al., 1998). In metamorphic geology, phase diagrams are routinely used to evaluate the absolute *P* and *T* recorded by mineral assemblages in rocks by locating the assemblage interpreted from thin section petrography as a mineral assemblage stability field on a phase diagram. A major advance in applying phase equilibria modelling to natural rocks is using isochemical, isobaric or isothermal phase diagrams (termed 'pseudosections') to explore the changes to mineral assemblages applicable to a single (rock) composition (Fig. 5a,b), or across a variety of rock compositions (Fig. 5c,d). These powerful diagrams can be used to explore geological processes. In addition to constraining conditions of peak metamorphism, recent studies have also used phase equilibria modelling to investigate prograde and retrograde metamorphism, partial melting and melt loss or melt addition, the role of water, metasomatism and alteration, mantle melting, and mineralization. Phase equilibria have also been used to model the behavior of accessory phases, as well as explore fundamental geodynamic and geochemical (re)cycling questions. Yakymchuk (2017) provides an excellent overview of recent applications of phase equilibria modelling in metamorphic geology, and some recent published examples are listed in Appendix 2.

The chemical systems used for phase equilibria modelling are continually evolving to provide closer approximations to the natural compositions of rocks. The chemical system Na_2O–CaO–K_2O–FeO–MgO–Al_2O_3–SiO_2–H_2O–TiO_2–O, abbreviated as NCKFMASHTO, is now used widely. Other components and elements that can be incorporated into phase equilibria modelling include MnO, Cr_2O_3, ZrO_2, Cl, S and C. Phase diagrams are now routinely applied to metasedimentary rocks, metabasaltic and intermediate to felsic intrusive rocks and more recently to ultramafic rocks and meteorites. Given an appropriate bulk (rock) composition and thermodynamic data, a pseudosection in a model chemical system can be calculated (Fig. 5). The most common variables used as axes for these diagrams are *P* and *T*. Within a *P–T* pseudosection (Fig. 5a),

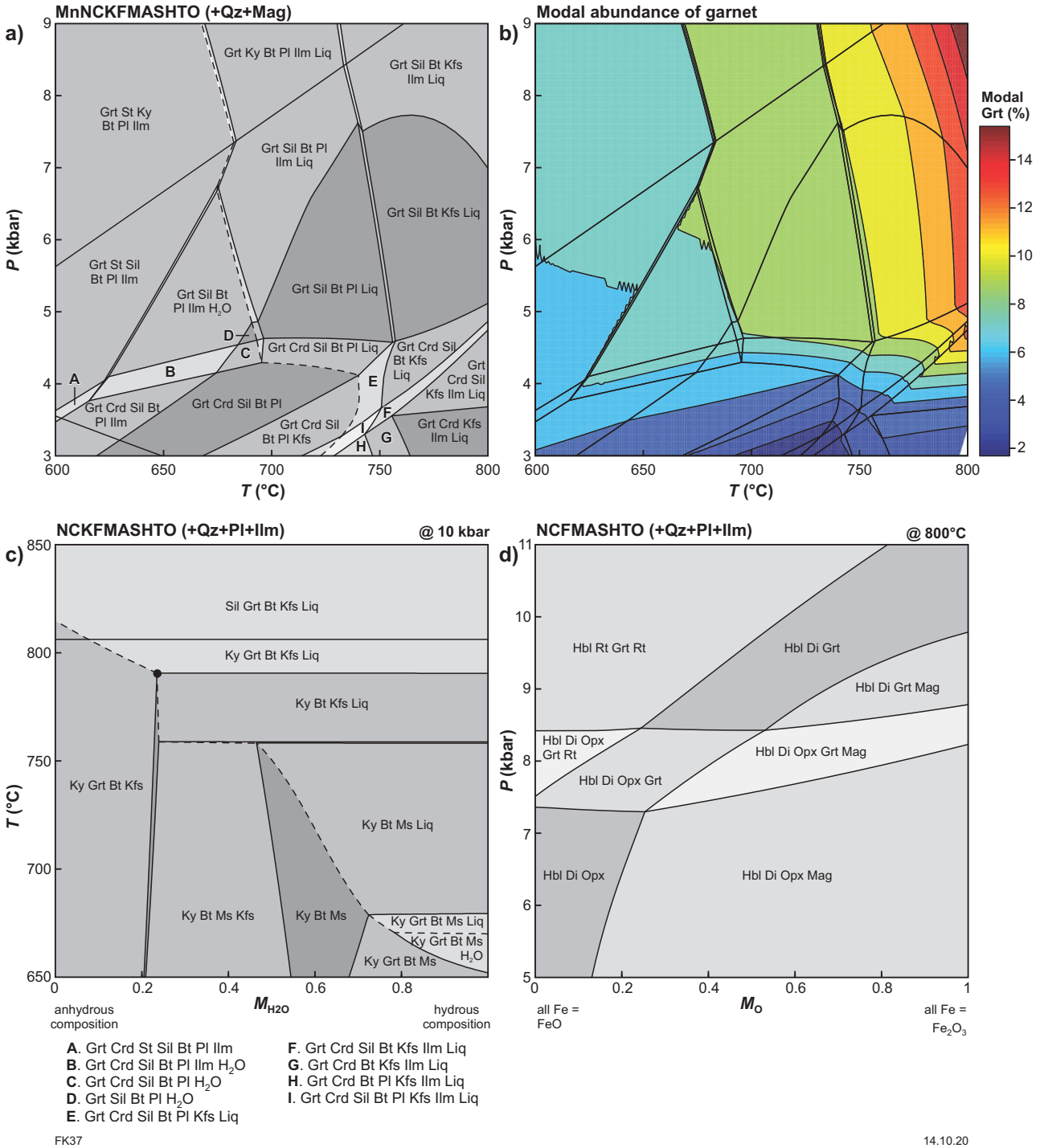

Figure 5. **Examples of calculated phase diagrams (pseudosections). All mineral abbreviations are defined in Appendix 3. Assemblage fields are shaded according to the number of degrees of freedom, with higher variance assemblages represented by darker shading: a) *P–T* pseudosection, in which mineral assemblages are shown as stability fields; b) mode isopleths of garnet (mol % ~ vol. %) from (a); c) *T*–M_{H2O} pseudosection calculated at 10 kbar, where M_{H2O} = amount of H_2O. The compositions across the x-axis range from a hydrous composition (0) to an anhydrous composition (1); d) *P*–M_O pseudosection calculated at 800°C, where M_O = amount of oxygen (for Fe_2O_3). The compositions across the x-axis range from a reduced composition with all Fe as FeO (M_{H2O} = 0) to an oxidized composition with all Fe as Fe_2O_3 (M_{H2O} = 1). Dashed line in (a) and (c) represents the solidus**

thermobarometric information can be retrieved from: i) the position in *P–T* space of the stability field that corresponds to a mineral assemblage interpreted from petrography; ii) the proportions (so-called 'modes') and compositions of the minerals in that field (Fig. 5b). Ideally, the mineral assemblage observed in the rock will coincide with a stable assemblage on a pseudosection, and the predicted modes and their compositions will be similar to observed values. Compositional phase diagrams can also be used to evaluate the stability of phases with changes in the chemical composition. These types of diagrams include *T*–composition (*X*) at a fixed *P* (Fig. 5c), *P–X* at a fixed *T* (Fig. 5d), and *X–X* at fixed *P* and *T*. Constructing phase diagrams that display equilibrium phase assemblages requires an understanding of the phase rule and of equilibrium thermodynamics (e.g. Powell, 1978; Spear, 1993) that is beyond the scope of this Record. There are several resources that provide good introductions to the fundamentals of phase equilibria including documentation on the **THERMOCALC** website, the **SERC Carleton** website and the textbooks by Spear (1993) and Vernon and Clarke (2008).

Phase equilibria modelling conducted by GSWA uses the software THERMOCALC version tc3xx (Powell and Holland, 1988, and recent updates) and the internally consistent thermodynamic dataset of Holland and Powell (2011; datasets tcds62 and 63). For selected samples, compositional and mode isopleths are calculated using the software TCInvestigator (Pearce et al., 2015; Fig. 5b). The chemical system used for the calculations is a necessary simplification of the more complex natural system, but it should include the key components that define the selected sample. Most rock compositions can be modelled in the 10-component NCKFMASHTO system. Manganese may also be included for subsolidus calculations because it can have an important effect on stabilizing some phases, such as garnet, to lower conditions as compared to a MnO-free system. Other chemical systems are used for appropriate samples. The software, dataset and *a–x* models are continuously being updated, and each Metamorphic History Record details the versions used for each individual sample. All files for calculations are available on the **THERMOCALC** website.

Bulk composition

The mineral assemblage observed in a metamorphic rock is primarily a result of the *P–T* conditions and the composition (*X*) of an appropriate scale of chemical equilibration. This composition is referred to as the 'equilibration volume' or more commonly the 'effective bulk composition' or simply 'bulk composition'. The volume of the effective bulk composition is ultimately controlled by chemical diffusion rates. Cation transport is typically faster and more efficient at higher *T*, and/or in the presence of intergranular volatiles or melt. For many samples, particularly those that have reached elevated *T* (above approximately 600°C), the effective bulk composition can be approximated by the whole-rock composition measured by X-ray fluorescence (XRF). However, some samples require a composition of a specific microstructure or domain to be calculated. These smaller-than-thin-section-scale bulk compositions can be obtained using compositional maps (e.g. EPMA or cropped TIMA) combined with mineral proportions and their chemistries. Most of the chemical components for phase equilibria modelling can be directly measured and converted into mole percentage for each oxide, the required input to THERMOCALC software. However, H_2O and Fe_2O_3 (for O) are two components that require different methodologies (discussed below). The techniques used to constrain the bulk composition for each sample are summarized in individual Metamorphic History Records.

Estimating the amount of H_2O

The amount of H_2O in the bulk composition will strongly influence the position of the solidus, as well as the *P–T* stabilities and proportions of H_2O-bearing phases, such as chlorite, micas and melt. An appropriate H_2O content in the bulk composition will allow for the peak mineral assemblage observed in the sample to be calculated as a stable field in the pseudosection, ideally with similar mineral modes and compositions. Methods for estimating an appropriate bulk H_2O content include:

- The loss on ignition (LOI) value from the whole-rock XRF composition. This technique measures other volatiles and should be regarded as a maximum value for H_2O
- Estimation based on the inferred H_2O content of H_2O-bearing minerals and their modal abundance in the rock
- H_2O saturation. Some samples can be assumed to have been saturated in H_2O during metamorphism. This assumption is commonly used for subsolidus rocks that have not experienced melting or melt loss, particularly metasedimentary protoliths, or for samples that may have been affected by fluids (e.g. hydrothermal/metasomatic rocks, rocks affected by fluid-present shearing)
- *P/T–*M_{H2O} diagrams. These diagrams investigate phase assemblage stabilities over a range of *P–T* conditions and H_2O contents (Fig. 5c). These diagrams are calculated at either fixed *P* or *T*, with H_2O content changing along the x-axis; M_{H2O} refers to the amount of H_2O, and is thus different from X_{H2O}, which is used for fluid composition. An appropriate H_2O content for the bulk composition is selected based on where in compositional (M_{H2O}) space the interpreted mineral assemblage occurs in the calculated diagram. These diagrams can also be used to assess the influence of H_2O on the location of phase-in and phase-out boundaries, which is equivalent to a sensitivity analysis of changing H_2O at a fixed *P* or *T*. The extent of H_2O contents used in *P/T–*M_{H2O} diagrams can range from low H_2O values (nominally anhydrous) to H_2O saturation, although the maximum values are generally defined by the LOI value.

Estimating the amount of Fe_2O_3

The amount of Fe_2O_3 can significantly modify the stabilities and proportions of Fe–Mg silicates and Fe–Ti oxides. An appropriate Fe_2O_3 content in the bulk composition will allow for the (peak) mineral assemblage observed in the sample to be calculated as a stable field in the pseudosection, ideally with similar mineral modes and compositions. For calculations performed with the

THERMOCALC software, the bulk Fe_2O_3 concentration must be converted to moles of FeO and O. That is, FeO as input to THERMOCALC is actually total Fe (i.e. FeO^T), and O expresses how many moles of Fe_2O_3 will be made from FeO. Therefore FeO^T moles = FeO + 2O, as for every mole of O two moles of FeO are required to make Fe_2O_3. Methods for estimating an appropriate Fe_2O_3 content include:

- FeO titration and Fe_2O_3 calculated by difference. The value determined by FeO titration is commonly an excellent approximation of the proportion of FeO:Fe_2O_3 in the bulk composition, and can easily be analysed in most geochemical laboratories. However, weathering and crushing during sample preparation can oxidize the sample, so the value obtained from FeO titration value should be treated as a maximum value for Fe_2O_3. A notable exception is for samples that contain abundant sulfides and have elevated SO_3 values. The oxidation of S^{2-} during the titration will reduce some of the Fe^{3+} in the sample, which may result in anomalously high Fe^{2+} values and apparent values of O and FeO that are too low and high, respectively. In these cases, the values may need to be corrected using alternative methods, as described below
- Estimation using mineral compositions. For many mineral analyses, Fe^{3+} can be calculated on the basis of stoichiometric mineral composition analyses, and the bulk Fe_2O_3 can be recalculated using those mineral compositions and their abundances. This approach is complicated when it involves hydrous Fe^{3+}-bearing minerals such as biotite and chlorite, as assumptions of stoichiometry in these minerals are commonly flawed
- An assumption of FeO:Fe_2O_3. Comparisons to similar samples and mineralogy with known or constrained FeO:Fe_2O_3 can be used. Typical values for Fe^{3+} are commonly set at 5–10% of total Fe, based on a consideration of the oxide–silicate mineralogy of the rock, although whether this estimate is applicable should be considered on a case-by-case basis
- *P/T*–X_{Fe2O3} diagrams (or *P/T*–X_O, *P/T*–M_O). These diagrams are used in a similar manner to the *P/T*–M_{H2O} diagrams described above (Fig. 5d). An appropriate O content for the bulk composition is selected based on where along the x-axis the interpreted mineral assemblage occurs in the calculated diagram. The O contents used in *P/T*–M_O diagrams can range from all Fe as Fe^{2+} to all Fe as Fe^{3+}, although the Fe^{3+} content determined from titration, if available, is typically a realistic maximum.

P–T–t path and interpretation

The *P–T–t* path of a metamorphic rock is the set of all *P–T* conditions to which a rock is subjected during its metamorphic history (Fig. 6). The trajectory and shape of the *P–T* path, the rates of metamorphic processes, and the duration of metamorphism are a function of the source of heat and, if *P* change occurs, the mechanisms of burial and uplift. An increase in *P* records burial of a rock to deeper crustal levels, whereas a *P* decrease implies that the rock has been uplifted (Fig. 6a). A *T* increase corresponds to a heating event, although heat can be internally derived through radiogenic heat production and does not necessarily require an external source. A decrease in *T* coincides with cooling. Therefore, the shape of the path, combined with *t* information, provides insight into the drivers of metamorphism, which commonly reflects the tectonic and/or geodynamic setting.

P–T paths can have a clockwise or anticlockwise geometry (Fig. 6b) that reflect fundamentally different styles of metamorphism and thus tectonothermal drivers. Unless otherwise defined, peak metamorphism corresponds to the maximum *T* (T_{max}) recorded by a rock (Fig. 6a).

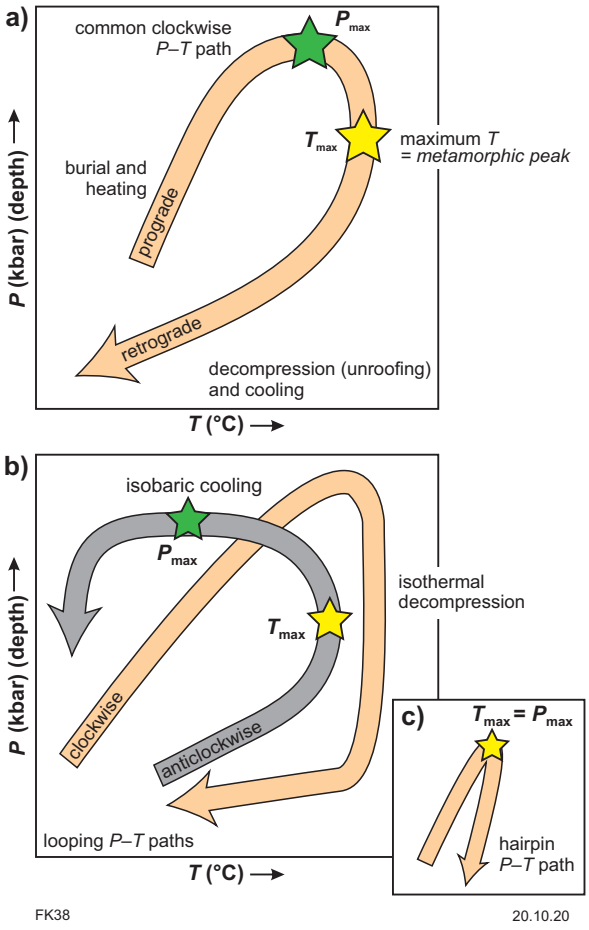

Figure 6. The different types and styles of *P–T* paths are clockwise, anticlockwise, looping and hairpin. Each path reflects the tectonic and/or geodynamic and erosion regime driving metamorphism: a) a common clockwise *P–T* path, with burial and heating along the prograde path and decompression and cooling on the retrograde path. This looping path reaches maximum *P* (P_{max}) before maximum *T* (T_{max}); b) clockwise and anticlockwise *P–T* paths. The anticlockwise path (grey arrow) reaches T_{max} before P_{max}, and shows a segment of cooling at near-constant *P* (isobaric cooling). The clockwise path (orange arrow) shows a segment of decompression at near-constant *T* (isothermal decompression); c) a hairpin *P–T* path has a similar prograde and retrograde history, and typically has coincident T_{max} and P_{max}

P–T paths with very similar pre-peak (prograde) and post-peak (retrograde) histories will have a tight hairpin loop and coincident maximum *P* (P_{max}) and T_{max} (Fig. 6c), regardless of the clockwise or anticlockwise trajectory. Looping clockwise paths involve an increase in *P* (with or without a significant increase in *T*) during the prograde history (Fig. 6b), recording burial of the rock to deeper levels in the crust, and the classification as clockwise is on the basis that *P–T* diagrams have *P* increasing up the y-axis. These types of *P–T* paths may reach P_{max} before the thermal peak, and commonly reflect regional metamorphism involving burial and subsequent conductive heating and erosion. Anticlockwise paths record an increase in *T* (with or without a significant increase in *P*) during the prograde history and may reach T_{max} before P_{max} (Fig. 6b). Similarly, classification as anticlockwise is on the basis that *P–T* diagrams have *P* increasing up the y-axis. Anticlockwise paths typically require an additional source of heat, such as magmatism. For both *P–T* path geometries, the retrograde path is characterized by a decrease in *T* and *P.* Some rocks may undergo unroofing at (near) constant *T*, resulting in an isothermal decompression segment of the *P–T* path, or cooling at (near) constant *P* as indicated by an isobaric cooling segment (Fig. 6b).

Constraining the *P–T* path

Reconstruction of the *P–T–t* path is a major objective in metamorphic studies (Fig. 7) due to the relationship of the shape of the *P–T* path and location of the path in *P–T* space with underlying (driving) tectonothermal processes. However, it is critical to appreciate that metamorphic rocks and mineral assemblages only ever preserve a small portion of the total *P–T* path due to the *t*-, *T*- and diffusion-dependent kinetics of mineral reactions. The *P–T* information is recorded by the assemblage comprising the major rock-forming minerals, whereas *t* can be retrieved from datable accessory minerals. Establishing the links between these variables in order to derive a *P–T–t* path is the goal of petrochronology. Most rocks contain some record of peak metamorphic conditions (~T_{max}) and the peak metamorphic mineral assemblage is typically identified on the basis of coarser grain size and/or spatial relationships of the coarse-grained minerals to each other. Equilibrium is most likely to have been reached at and near the metamorphic peak. For some rocks, the conditions of peak metamorphism are the only part of the *P–T* path that is preserved, with little modification to the minerals as the rock cooled. Such rocks are not useful, in isolation, for constraining a more complete evolution of the *P–T* path. However, some rocks record a composite of mineral assemblages from the prograde, peak and retrograde segments of the overall history and are therefore particularly useful for constraining the *P–T* path. Rocks that have a sedimentary or volcanic protolith can be inferred to have originated at Earth's surface prior to metamorphism, been buried to develop and record metamorphic mineral assemblages, and then exhumed to the surface (where sampling occurs), and the metamorphic assemblages will offer the most robust constraints on the overall evolution. In practice, the *P–T–t* path is typically constrained by use of numerous rocks with different bulk compositions and metamorphic mineral assemblages from a single terrane or tectonic domain. Ideally, several lines of evidence from either a single sample or multiple samples will converge towards a common interpretation.

There are various methods that can be used to reconstruct parts of a *P–T* path. Inclusions of minerals retained in host minerals can be useful for inferring a sequence of growth along a *P–T* trajectory, particularly for minerals that have relatively restricted *P–T* stabilities. However, the included phase may have been stable prior to or during the growth of the host mineral, so the crystallization history is not necessarily unequivocal. The most that can be established is that the mineral inclusion plus the host were stable together. Trends in mineral compositions in compositionally zoned minerals can also be used to constrain segments of the *P–T* path. Domains with different chemistries correspond to growth at different *P–T* conditions either from a single evolving event or even separate events. A common zoning pattern shows a difference in composition between the centre of a mineral (core) compared to its rim (Fig. 7b), and concentric domains of different compositions arranged between the core and the rim. Minerals that typically show this type of zoning in major and/or trace elements include garnet and plagioclase, and at lower *T* mica and amphibole. Importantly, the absence of zoning does not necessarily imply a simple history or growth at similar metamorphic conditions. At elevated *T* (e.g. >>600°C for garnet; Caddick et al., 2010) and sufficient duration, zoning may be homogenized as intracrystalline diffusion becomes more effective at eliminating compositional variation. The chemistries of matrix minerals are likely to record the *P–T* conditions at which the metamorphic fabric was developed or to which it was reset during cooling (depending on the peak metamorphic temperature), or the conditions of an overprinting event/s.

Some rocks contain evidence for incomplete metamorphic reactions or other textural evidence from which a mineral growth sequence can be inferred. A simple example is the transformation of one polymorph mineral to another. This type of replacement is most common in the aluminosilicate (Al_2SiO_5) polymorphs, such as andalusite replaced by sillimanite. Some minerals are completely consumed along the *P–T* path, although the shape of the reactant grain may be preserved as pseudomorphs and the metamorphic reaction can be identified. An example of a more complex incomplete reaction texture involves the formation of coronas, which consist of one or more rims of a mineral or minerals around a central reactant phase. Coronas can also involve the fine-scale intergrowth of minerals in a texture known as symplectite.

Worked example (clockwise *P–T* path)

Figure 7 illustrates a hypothetical clockwise *P–T* path and the types of data discussed above that can be used to reconstruct that path. The *P–T* path has segments that are recorded in the rock (thick lines), whereas other segments must be inferred (dashed lines). This example is a metasedimentary rock that must have been deposited at the surface, and detrital zircon ages provide constraints on the timing of deposition (M0, blue star in Fig. 7a). A simplified phase diagram with key mineral assemblages (+Qz+Ilm+H_2O±Pl) is shown in Figure 7a. The thick grey lines represent boundaries across which a phase appears or disappears relative to the clockwise *P–T* path. This diagram is constructed specifically for the bulk composition of this sample. The only evidence for the prograde history is the chemistry of the garnet cores that preserve high Ca values

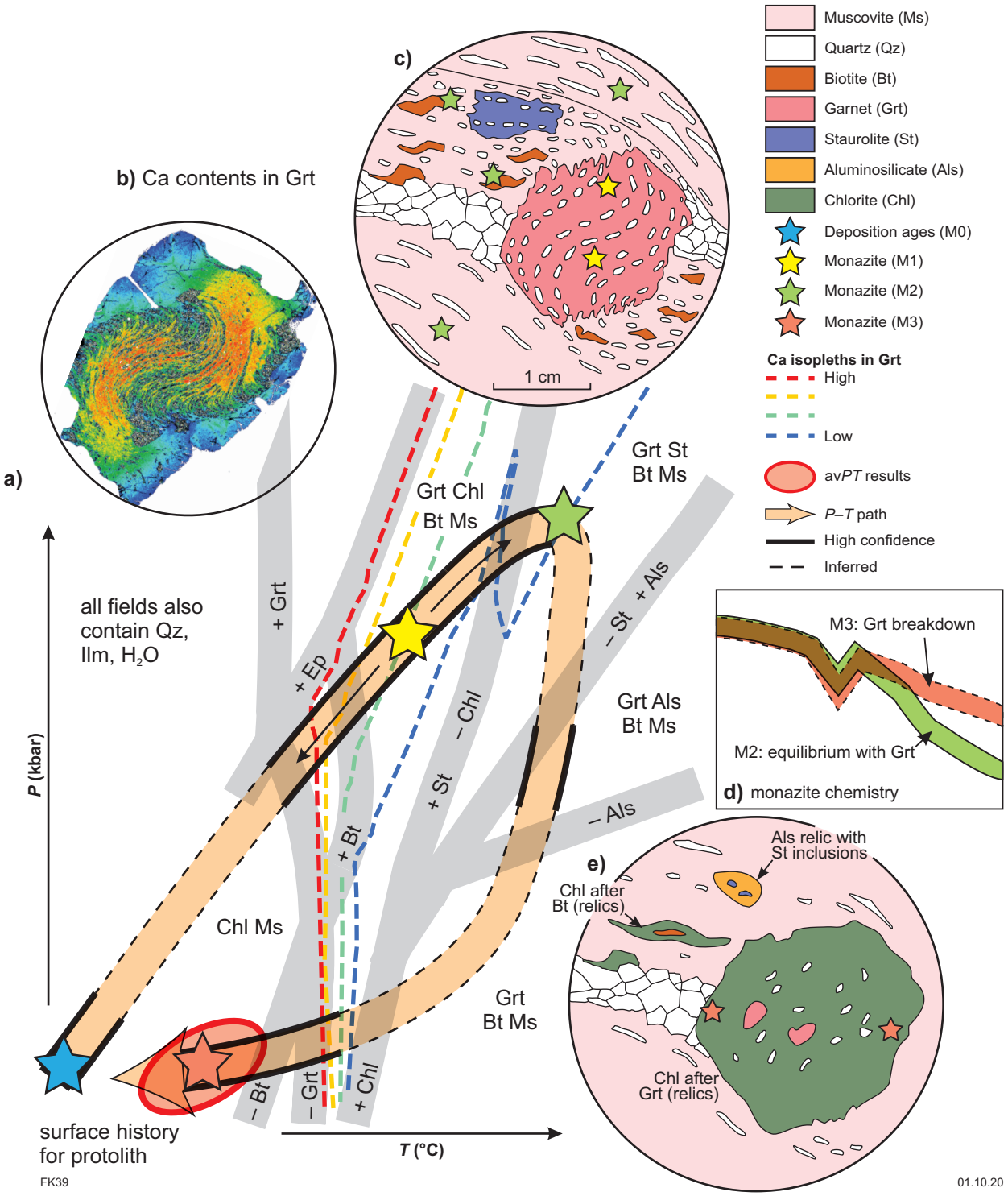

Figure 7. **Hypothetical clockwise *P–T* path (orange arrow) for a metasedimentary rock with segments recorded in the rock (thick lines) and inferred (dashed lines): a) simplified phase diagram with key mineral assemblages (+Qz+Ilm+H_2O±Pl); b) Ca elemental map from garnet porphyroblast; Ca isopleths shown as thick dashed lines on (a) that correspond to same colour as the Ca map; c) schematic diagram of the peak metamorphic assemblage (Grt–St–Bt–Ms+Qz+Ilm+H_2O±Pl field). Yellow stars depict monazite inclusions in garnet that date the timing of prograde metamorphism (M1); green stars are monazite grains aligned in the fabric that date peak metamorphism (M2); d) schematic trace element plot of M2 and M3 (described below) monazite. Diagram unlabelled for clarity; see Fig. 2; e) textural evolution associated with the retrograde path. Red ellipse shows the *P–T* estimate based on multiple-reaction thermobarometry (avPT calculation in THERMOCALC; see Fig. 4b) using mineral compositions from the matrix assemblage of Chl–Ms+Qz+Ilm+H_2O±Pl. See text for further details**

(red zoning in Fig. 7b) and the inclusions (Qz+Chl+Ms). There is no evidence that epidote was stable, constraining the prograde path within the Chl–Ms (+Qz+Ilm+H_2O±Pl) fields, below the pressures that epidote is stable. The peak and retrograde metamorphic history is recorded by the preserved minerals and their textures. The abundance of minerals across any *P–T* diagram can also be contoured, so that the relative growth and consumption of minerals along a *P–T* path can be evaluated (not shown on Fig. 7a). Coarse-grained garnet and staurolite porphyroblasts occur within a matrix of biotite, muscovite and quartz. The foliation can be followed into the garnet rims and through the staurolite porphyroblasts (Fig. 7c), suggesting that these phases were growing and the fabric was developing at the same time near and at peak metamorphic conditions within the Grt–St–Bt–Ms (+Qz+Ilm+H_2O±Pl) field. The predicted Ca compositions of garnet have steep slopes in *P–T* space (dashed coloured lines, Fig. 7a), which can be used to infer temperature conditions during growth. The decrease in Ca from core to rim in the garnet porphyroblasts (red to blue zoning in Fig. 7b) support an increase in temperature (with or without an increase in pressure), and the Ca content of the garnet rims is the same as the predicted value in the peak field (blue dashed line, Fig. 7a). The small yellow stars in Figure 7c depict monazite inclusions in garnet, and their ages record the timing of prograde metamorphism (M1), which could occur anywhere along the prograde path where garnet was growing (yellow star and associated arrows on *P–T* path, Fig. 7a). The small green stars in Figure 7c represent monazite grains that are aligned in the fabric, and their ages record the timing of peak metamorphism (M2). The relationship between the timing of monazite growth and the behaviour of major rock-forming minerals, such as garnet, can be further evaluated using monazite trace element chemistry. Figure 7d shows a schematic trace element plot of M2 and M3 (described below) monazite. The green solid field is the range of chemistry of M2 monazite, which is in equilibrium with garnet and has low HREE contents (right side of Fig. 7d). The red dashed field is the range of chemistry of M3 monazite associated with garnet breakdown, which has higher concentrations of HREE that were liberated from garnet and incorporated into newly growing monazite. In this example, the matrix also contains rare relics of aluminosilicate that are mostly replaced by muscovite, and host very small rounded inclusions of staurolite (Fig. 7e). These relationships indicate the growth of aluminosilicate at the expense of staurolite during a decrease in pressure from peak conditions, represented by the thick segment of the *P–T* path within the Grt–Als–Bt–Ms (+Qz+Ilm+H_2O±Pl) field. Garnet breakdown with a decrease in *P* and *T* results in the growth of chlorite that pseudomorphs former garnet porphyroblasts, preserving only small garnet relics. This texture corresponds to the crossing of the '+Chl' boundary at the lower *P* portion of Figure 7a. Small inclusions of monazite (pink stars in Fig. 7e) within the chlorite pseudomorphs can be used to date the timing of this lower grade assemblage. Chlorite also grows at the expense of biotite as *T* decreases, resulting in small relics of biotite within matrix chlorite. The red ellipse on Figure 7a shows the *P–T* estimate based on multiple-reaction thermobarometry (avPT calculation in THERMOCALC; see Fig. 4b) using mineral compositions from the matrix assemblage of Chl–Ms (+Qz+Ilm+H_2O±Pl).

Apparent thermal gradients and tectonic setting

The apparent thermal gradient is defined as the *T* change with depth and can offer critical constraints to plausible tectonic settings of metamorphism (Fig. 8). Because metamorphism is primarily a thermally driven process, apparent thermal gradient information provides a first-order constraint on the regional thermal regime of the crust and mantle lithosphere. This, in turn, offers insight into the driver/s and tectonic or geodynamic regime causing the metamorphism, because different tectonic regimes have different thermal characteristics. The regional thermal regime is fundamentally a balance between the advection vs conduction of heat within a metamorphic system. The term 'apparent thermal gradient' means that the gradient is linear in *P–T* space, unlike the actual geotherm, and so is an approximation for the characterization of the thermal regime of the Earth's crust. There are various ways to calculate the apparent thermal gradient from metamorphic data, but the most straightforward calculation is simply the *T*/*P* ratio of the peak metamorphic conditions. Quoting of apparent thermal gradients in °C/kbar negates the need to convert *P* to depth (based on inferred density) and so is preferred. Apparent thermal gradients cooler than the normal geotherm (45°C/kbar) occur in settings that are dominated by the advection of heat and material and are typically attributed to subduction zones. Gradients between 45 and 150°C/kbar indicate a more equal balance between heat conduction and heat advection. These gradients correspond to high *T*/*P* 'Barrovian' metamorphism, and broadly demonstrate a conductive response to thickening, as expected within a typical collisional orogenic belt.

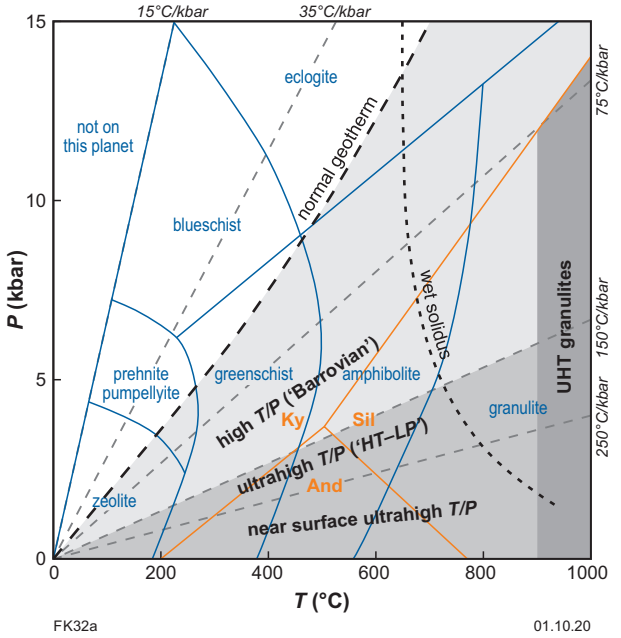

Figure 8. ***P–T* diagram with apparent thermal gradients that can be used to infer tectonic setting. The normal (conductive) continental geotherm ('normal geotherm') is shown at 45°C/kbar (Stüwe, 2007). Metamorphic facies and aluminosilicate stability fields are also shown. Adapted from Kelsey and Hand (2015)**

Apparent thermal gradients >150ºC/kbar ('ultrahigh *T/P*') are dominated by heat conduction in settings that may be pervaded by magma, and may involve crustal extension, thermal blanketing and/or mantle underplating. Apparent thermal gradients >250ºC/kbar imply near surface conditions ('near surface ultrahigh *T/P*').

Uncertainties

The techniques outlined in this Record aim to help characterize and understand complex natural systems. However, the reduction of natural systems into simpler model systems will introduce uncertainties that can affect the results and interpretations. Analytical (or systematic) uncertainties in *P–T* calculations include: i) uncertainty associated with thermodynamic calculations, including the parameters used in the *a–x* models and the dataset (e.g. Powell and Holland, 2008); ii) uncertainty associated with data collection, such as whole-rock geochemistry, mineral chemistry and geochronological age data.

Other types of uncertainty are more difficult to quantify. For a complex history, identifying from petrographic analysis the changes in a mineral assemblage with evolving *P–T* conditions and determining the phases in equilibrium at any stage during metamorphism can be particularly challenging. Identification of the peak vs retrograde assemblages requires careful study of the spatial relationships between minerals, as well as taking into account factors such as grain size, mineral orientation (e.g. number of tectonic fabrics) and knowledge of the *P–T* stability of different minerals. Therefore, spatiotextural and compositional data are key to providing confidence in the interpretation of different stages of the recorded metamorphic evolution, although it must be considered that these features can be subsequently modified and as such may not retain their equilibrium characteristics. A broad example of this approach is that, in general, retrograde assemblages feature more hydrous minerals than the peak metamorphic assemblage, owing to the fact that minerals that are stable at lower *T* are typically more hydrous than higher *T* minerals. Metamorphic reactions also may not proceed at the *P–T* conditions predicted from phase equilibria modelling due to kinetic barriers related to nucleation, interface reaction (dissolution and growth) and intergranular transport of cations. Kinetic barriers to nucleation are generally considered to be the dominant rate-limiting step in metamorphic assemblages attaining equilibrium. These disequilibrium processes can result in the preservation of metastable reactants outside their predicted *P–T* stabilities, which can affect petrographic interpretations. Beyond petrography, another potentially significant source of uncertainty associated with pseudosection thermobarometry is determining the scale of equilibration and choosing an effective bulk composition. For many samples, the measured whole-rock composition is used for the effective bulk composition, which implies that the analysed rock volume achieved chemical equilibrium. However, establishing that a mineral assemblage has reached equilibrium is not trivial and will be subject to interpretation.

There must also be an understanding of what part of the *P–T* evolution a bulk composition might record. Any modelled bulk composition used to constrain peak metamorphic *P–T* conditions carries the assumption that the bulk composition was not modified beyond the metamorphic peak. This assumption will not be appropriate for rocks that have subsequently undergone hydrothermal retrogression. There may also be significant differences between a protolith composition and a metamorphic composition, particularly for high-grade rocks that have experienced partial melting and melt loss. In this case, a residual composition can be used to constrain peak *P–T* conditions and segments of the retrograde path. However, that composition will not be appropriate for investigating the history prior to melt loss. Inverse modelling has been used to add melt back into the bulk composition while progressing down *T*, but this technique requires assumptions about the *P–T* trajectory of the prograde path and the melt composition, which are not always clear. Therefore, the effective bulk composition can and does change along a *P–T* trajectory, with melt loss being one of those reasons. Other ways for the effective bulk composition to change along a *P–T* trajectory involve the partitioning of cations into growing porphyroblasts (e.g. Mn into garnet), resulting in the cores of zoned minerals not being in equilibrium (or even participating) with the surrounding phase assemblage. In some cases, this can be examined by forward modelling of porphyroblast growth.

Inevitably there are discrepancies between the actual chemical system appropriate for a rock and the one used in the models. Fundamental components that cannot easily be measured, such as H_2O and Fe_2O_3, will have more uncertainty compared to other major components, although sensitivity analysis through the construction of *P/T–X* diagrams will offer some degree of uncertainty assessment. The presence of components that are not incorporated into existing *a–x* models will affect the predicted stabilities of some phases. For example, the presence of Zn in phases such as staurolite or spinel will expand the stability of these phases to lower *P* and *T* in nature in comparison with the predictions. Similarly, the presence of Cl or F in biotite will stabilize it to higher *T* in comparison with calculated models.

The most significant uncertainty in linking age data to *P–T* data concerns where along the *P–T* path the age data reflects. Petrochronology is concerned with constraining which major and accessory minerals were exchanging elements with each other as a way to constrain whether the major mineral (commonly garnet) was growing or breaking down — that is, taking in or liberating trace elements — which, in turn, can be linked to changes in *P–T*. However, whereas trace element trends can be identified in major and accessory minerals in empirical datasets from natural rocks, the science of linking the growth or breakdown of the two, and thus age data, remains imperfect. This complexity is partly because the growth and breakdown of accessory minerals remain imperfectly understood as a function of *P* and *T*, and partly also because the growth and breakdown of accessory minerals may not always follow classic equilibrium thermodynamic principles (e.g. Nemchin et al., 2001).

The potential limitations discussed above need to be considered when applying the results of phase equilibria modelling to natural rocks and constraining *P–T–t* paths. Nevertheless, in many examples, the equilibrium approach to metamorphic studies, and the petrochronological

approach to integrating age data, reproduces many first-order observations from natural rocks, and this methodology can be used to address various geological questions in a relatively fast and cost-effective way.

Summary

The rock record preserves evidence of the geological processes that have shaped the Earth and its resources. The metamorphic cycle involves burial (increasing *P* and *T*) and exhumation (decreasing *P* and *T*) of terranes in response to tectonothermal processes. Phase equilibria modelling and improved thermobarometry enable us to retrieve quantitative *P–T* conditions from metamorphic rocks with a high degree of confidence, largely owing to the graphical depiction of fields of mineral assemblage stability in *P–T* space. Thermobarometric data can now be integrated with age information to reconstruct the *P–T–t* path followed by individual rocks and units. The apparent thermal gradients calculated from *P–T* data relate directly to the thermal regime at the time of metamorphism, which can be used to infer geodynamic setting and heat source. The overall shape of the *P–T–t* path is a function of the relative rates of burial and heating vs cooling and exhumation. Together these data can be used to define the sequence of geologic events and tectonothermal drivers responsible for the evolution of these terranes.

References

Armstrong, JT 1988, Quantitative analysis of silicate and oxide minerals: Comparison of Monte Carlo, ZAF and phi-rho-z procedures, v. 23, p. 239–246.

Berman, RG 1988, Internally-consistent thermodynamic data for minerals in the system NaO–KO–CaO–MgO–FeO–FeO–AlO–SiO–TiO–HO–CO: Journal of Petrology, v. 29, p. 445–522.

Caddick, MJ, Konopásek, J and Thompson, AB 2010, Preservation of Garnet Growth Zoning and the Duration of Prograde Metamorphism: Journal of Petrology, v. 51, no. 11, p. 2327–2347, doi:10.1093/petrology/egq059.

Holland, TJB and Powell, R 1998, An internally consistent thermodynamic data set for phases of petrological interest: Journal of Metamorphic Geology, v. 16, no. 3, p. 309–343.

Holland, TJB and Powell, R 2011, An improved and extended internally consistent thermodynamic dataset for phases of petrological interest, involving a new equation of state for solids: Journal of Metamorphic Geology, v. 29, no. 3, p. 333–383.

Kelsey, DE and Hand, M 2015, On ultrahigh temperature crustal metamorphism: Phase equilibria, trace element thermometry, bulk composition, heat sources, timescales and tectonic settings: Geoscience Frontiers, v. 6, no. 3, p. 311–356, doi:10.1016/j.gsf.2014.09.006.

Lu, YJ, Fielding, IOH and Wingate, MTD 2020, Introduction to geochronology information 2020: Geological Survey of Western Australia, 8p.

Nemchin, AA, Giannini, S, Bodorkos, S and Oliver, NHS 2001, Ostwald ripening as a possible mechanism for zircon overgrowth formation during anatexis: Theoretical constraints, a numerical model, and its application to pelitic migmatites of the Tickalara Metamorphics, northwestern Australia: Geochimica et Cosmochimica Acta, v. 65, no. 16, p. 2771–2787.

Pearce, MA, White, AJR and Gazley, MF 2015, TCInvestigator: automated calculation of mineral mode and composition contours for thermocalc pseudosections: Journal of Metamorphic Geology, v. 33, no. 4, p. 413–425, doi:10.1111/jmg.12126.

Powell, R 1978, Equilibrium Thermodynamics in Petrology, An Introduction: Harper & Row Ltd, London, 284p.

Powell, R and Holland, TJB 1988, An internally consistent dataset with uncertainties and correlations: 3. Applications to geobarometry, worked examples and a computer program: Journal of Metamorphic Geology, v. 6, no. 2, p. 173–204.

Powell, R and Holland, TJB 1994, Optimal geothermometry and geobarometry: American Mineralogist, v. 79, no. 1–2, p. 120–133.

Powell, R and Holland, TJB 2008, On thermobarometry: Journal of Metamorphic Geology, v. 26, no. 2, p. 155–179.

Powell, R, Holland, TJB and Worley, BA 1998, Calculating phase diagrams involving solid solutions via non-linear equations, with examples using THERMOCALC: Journal of Metamorphic Geology, v. 16, p. 577–588.

Spear, FS 1993, Metamorphic phase equilibria and pressure–temperature–time paths: Mineralogical Society of America, Monograph, 799p.

Stüwe, K 2007, Geodynamics of the lithosphere: An introduction: Springer, Berlin, 493p.

Vernon, RH and Clarke, GL 2008, Principles of Metamorphic Petrology: Cambridge University Press, 478p.

White, RW, Powell, R, Holland, TJB, Johnson, TE and Green, ECR 2014a, New mineral activity–composition relations for thermodynamic calculations in metapelitic systems: Journal of Metamorphic Geology, v. 32, no. 3, p. 261–286.

White, RW, Powell, R and Johnson, TE 2014b, The effect of Mn on mineral stability in metapelites revisited: New a-x relations for manganese-bearing minerals: Journal of Metamorphic Geology, doi:10.1111/jmg.12095.

Whitney, DL and Evans, BW 2010, Abbreviations for Names of Rock-Forming Minerals: American Mineralogist, v. 95, p. 185–187.

Yakymchuk, C 2017, Applying Phase Equilibria Modelling to Metamorphic and Geological Processes: Recent Developments and Future Potential: Geoscience Canada, v. 44, no. 1, p. 27, doi:10.12789/geocanj.2017.44.114.

Appendix 1

Summary of workflow for standard metamorphic study

1. **Sample selection**. Metamorphic studies aim to address specific geological questions. Samples must have a broader geologic context that demonstrates they can further our understanding of the evolution of a tectonic or stratigraphic unit. Detailed petrography is used to identify the peak assemblage, and if possible, any information on the prograde or retrograde evolution. Ideally the inferred phase assemblage/s will comprise a group of minerals that, when considered together, have a relatively limited *P–T* stability that will provide meaningful metamorphic constraints. Samples are selected based on mineral assemblage, presence of datable accessory phases and pertinent field observations.

2. **Acquire polished thin section/s and whole-rock chemistry.** Care is taken to ensure that the thin section and the sample volume selected for whole-rock chemistry are close in terms of featuring the same minerals and no significant compositional differences (e.g. in the amount of porphyroblasts and/or leucosomes and/or micaceous layers in one sample volume vs the other). Relatively small samples are commonly used for whole-rock geochemical analysis (generally <<2 kg). Whole-rock chemistry for most samples includes Fe titration for $FeO:Fe_2O_3$.

3. **Collect TIMA data for polished thin section(s) and process data using GSWA guidelines.** These data are used to confirm mineralogy and estimate modal abundance of all phases, evaluate textures and microstructures preserved in the thin section, and to identify datable accessory phases (i.e. monazite) and their grain context in relation to other rock-forming minerals.

At this stage, the metamorphic (thermobarometric) and age (geochronology) data are acquired separately. After these data are obtained and processed, the final *P–T–t* data are defined. Additional analytical details for the geochronology and any trace element data collected simultaneously are provided in the Introduction to Geochronology Information document released each year on the parent data package (e.g. Lu et al., 2020).

4. **In situ geochronology workflow**

   a) Monazite is the primary accessory mineral that is used by GSWA to date metamorphism, although depending on P–T–X conditions, titanite, zircon or xenotime may also be used. Selected monazite grains are characterized using BSE images. Parameters assessed include petrographic setting, grain size and shape, the occurrence of alteration or cracks, compositional zoning, and the presence and mineralogy of inclusions. These images are typically collected with a TESCAN MIRA-3 SEM at the John de Laeter Centre at Curtin University in Perth, Western Australia. For some samples, selected monazite grains may be further characterized via collection of element maps with the EPMA.

   b) Collection of U–Th–Pb age data, typically with LA-ICP-MS at the John de Laeter Centre. For selected samples, trace element chemistry of monazite grains may be acquired simultaneously LASS methods or separately using a quadrupole ICP-MS or a EPMA.

   c) Process U–Th–Pb age data. Time-resolved mass spectra are reduced in Iolite 4 (Paton et al., 2011). The isotope ratios and their propagated uncertainties are exported from Iolite and then used to calculate dates in Isoplot 3.71 (Ludwig, 2003). Ideally, age components are defined based on a weighted mean date, although if the data do not define a statistically robust weighted mean, the age spread will be reported. If trace element data are collected simultaneously with LASS, these data are also reduced in Iolite, and the software **ioGAS** is used to evaluate chemistry and assign geochemical groups.

5. **Phase equilibria modelling workflow**

   Most *P–T* estimates for samples analysed by GSWA are based on the results of phase equilibria modelling, although other thermobarometric techniques may also be used. The thermobarometric methods used for each sample will be summarized in individual Metamorphic History Records. The workflow outlined here pertains to phase equilibria modelling.

   a) Determine the most appropriate bulk composition for the sample and assemblage.

   b) Acquire mineral chemistry or elemental maps, if these data are to be collected.

   c) Calculate appropriate *P–T–X* pseudosections based on the scientific question(s) to be addressed. The *P–T* pseudosection is typically the final diagram that is used to constrain metamorphic conditions. However, *P/T–X* diagrams can also be useful to calculate prior to the *P–T* pseudosection, particularly for the following applications: i) to determine the most appropriate bulk composition for the calculation of *P–T* pseudosections, particularly regarding H_2O and Fe_2O_3; ii) to conduct a sensitivity analysis for

various components with higher uncertainty, such as H_2O and Fe_2O_3; iii) to investigate the barometric or thermal evolution across changing composition (e.g. melt loss or alteration). Contour the pseudosections for mineral modes and mineral chemistry.

d) Compare the metamorphic assemblage(s) interpreted from petrographic analysis and mineral chemistry with the fields shown in calculated pseudosections to constrain as much of the *P–T* evolution as possible.

e) Integrate the results of in situ geochronology with the *P–T* path using textural and chemical information (if available).

References

Lu, YJ, Fielding, IOH and Wingate, MTD 2020, Introduction to geochronology information 2020: Geological Survey of Western Australia, 8p.

Ludwig, KR 2003, Isoplot 3.00; A geochronological toolkit for Microsoft Excel: Berkeley Geochronology Centre, Special Publication 4, 70p.

Paton, C, Hellstrom, J, Paul, B, Woodhead, J and Hergt, J 2011, Iolite: freeware for the visualization and processing of mass spectrometer data: Journal of Analytical Atomic Spectrometry, v. 26, p. 2508–2518.

Appendix 2

Bibliography with seminal references and some published examples

In situ geochronology and petrochronology

Metamorphic zircon growth

Kohn, MJ, Corrie, SL and Markley, C 2015, The fall and rise of metamorphic zircon: American Mineralogist, v. 100, no. 4, p. 897–908, doi:10.2138/am-2015-5064.

Kohn, MJ and Kelly, NM 2017, Petrology and Geochronology of Metamorphic Zircon, *in* Microstructural geochronology: Planetary Records Down to Atom Scale *edited by* DE Moser, F Corfu, JR Darling, KT Tait and SM Reddy: John Wiley and Sons Inc: Geophysical Monograph, p. 35–61.

Metamorphic monazite growth

Corrie, SL and Kohn, MJ 2008, Trace-element distributions in silicates during prograde metamorphic reactions: implications for monazite formation: Journal of Metamorphic Geology, v. 26, no. 4, p. 451–464, doi:10.1111/j.1525-1314.2008.00769.x.

Goswami-Banerjee, S and Robyr, M 2015, Pressure and temperature conditions for crystallization of metamorphic allanite and monazite in metapelites: a case study from the Miyar Valley (high Himalayan Crystalline of Zanskar, NW India): Journal of Metamorphic Geology, v. 33, no. 5, p. 535–556, doi:10.1111/jmg.12133.

Harlov, DE, Wirth, R and Hetherington, CJ 2011, Fluid-mediated partial alteration in monazite: the role of coupled dissolution–reprecipitation in element redistribution and mass transfer: Contributions to Mineralogy and Petrology, v. 162, no. 2, p. 329–348, doi:10.1007/s00410-010-0599-7.

Högdahl, K, Majka, J, Sjöström, H, Nilsson, KP, Claesson, S and Konečný, P 2012, Reactive monazite and robust zircon growth in diatexites and leucogranites from a hot, slowly cooled orogen: implications for the Palaeoproterozoic tectonic evolution of the central Fennoscandian Shield, Sweden: Contributions to Mineralogy and Petrology, v. 163, no. 1, p. 167–188, doi:10.1007/s00410-011-0664-x.

Kohn, MJ and Malloy, MA 2004, Formation of monazite via prograde metamorphic reactions among common silicates: implications for age determinations: Geochimica et Cosmochimica Acta, v. 68, no. 1, p. 101–113, doi:10.1016/S0016-7037(03)00258-8.

McFarlane, CRM, Connelly, JN and Carlson, WD 2006, Contrasting response of monazite and zircon to a high-T thermal overprint: Lithos, v. 88, 1-4, p. 135–149, doi:10.1016/j.lithos.2005.08.008.

Pyle, JM and Spear, FS 2003, Four generations of accessory-phase growth in low-pressure migmatites from SW New Hampshire: American Mineralogist, v. 88, p. 338–351.

Rubatto, D, Chakraborty, S and Dasgupta, S 2013, Timescales of crustal melting in the Higher Himalayan Crystallines (Sikkim, Eastern Himalaya) inferred from trace element-constrained monazite and zircon chronology: Contributions to Mineralogy and Petrology, v. 165, no. 2, p. 349–372, doi:10.1007/s00410-012-0812-y.

Seydoux-Guillaume, A-M, Paquette, J-L, Wiedenbeck, M, Montel, JM and Heinrich, W 2002, Experimental resetting of the U–Th–Pb systems in monazite: Chemical Geology, v. 191, p. 165–181.

Williams, ML, Jercinovic, MJ, Harlov, DE, Budzyń, B and Hetherington, CJ 2011, Resetting monazite ages during fluid-related alteration: Chemical Geology, v. 283, 3–4, p. 218–225, doi:10.1016/j.chemgeo.2011.01.019.

Wing, BA, Ferry, JM and Harrison, TM 2003, Prograde destruction and formation of monazite and allanite during contact and regional metamorphism of pelites: Petrology and geochronology: Contributions to Mineralogy and Petrology, v. 145, p. 228–250.

Petrochronology

Engi, M 2017, Petrochronology Based on REE-Minerals: Monazite, Allanite, Xenotime, Apatite: Reviews in Mineralogy and Geochemistry, v. 83, no. 1, p. 365–418, doi:10.2138/rmg.2017.83.12.

Gromet, LP and Silver, LT 1983, Rare earth element distributions among minerals in a granodiorite and their petrogenetic implications: Geochimica et Cosmochimica Acta, v. 47, p. 925–939.

Hacker, B, Kylander-Clark, A and Holder, R 2019, REE partitioning between monazite and garnet: Implications for petrochronology: Journal of Metamorphic Geology, v. 37, no. 2, p. 227–237, doi:10.1111/jmg.12458.

Kelsey, DE, Clark, C and Hand, M 2008, Thermobarometric modelling of zircon and monazite growth in melt-bearing systems: Examples using model metapelitic and metapsammitic granulites: Journal of Metamorphic Geology, v. 26, p. 199–212.

Kohn, MJ, Engi, M and Lanari, P (editors) 2017, Petrochronology: Methods and Applications: Mineralogical Society of America, Reviews in Mineralogy and Geochemistry 83, 596p.

Mottram, CM, Warren, CJ, Regis, D, Roberts, NMW, Harris, NBW, Argles, TW and Parrish, RR 2014, Developing an inverted Barrovian sequence; insights from monazite petrochronology: Earth and Planetary Science Letters, v. 403, p. 418–431, doi:10.1016/j.epsl.2014.07.006.

Rubatto, D 2002, Zircon trace element geochemistry: partitioning with garnet and the link between U–Pb ages and metamorphism: Chemical Geology, v. 184, p. 123–138.

Rubatto, D, Hermann, J and Buick, IS 2006, Temperature and Bulk Composition Control on the Growth of Monazite and Zircon During Low-pressure Anatexis (Mount Stafford, Central Australia): Journal of Petrology, v. 47, no. 10, p. 1973–1996, doi:10.1093/petrology/egl033.

Taylor, RJM, Harley, SL, Hinton, RW, Elphick, S, Clark, C and Kelly, NM 2015, Experimental determination of REE partition coefficients between zircon, garnet and melt: a key to understanding high-T crustal processes: Journal of Metamorphic Geology, v. 33, no. 3, p. 231–248, 18p., doi:10.1111/jmg.12118.

Yakymchuk, C, Clark, C and White, RW 2017, Phase Relations, Reaction Sequences and Petrochronology: Reviews in Mineralogy and Geochemistry, v. 83, no. 1, p. 13–53, doi:10.2138/rmg.2017.83.2.

Thermobarometry

Thermodynamic equilibrium

Powell, R and Holland, T 2010, Using Equilibrium Thermodynamics to Understand Metamorphism and Metamorphic Rocks: Elements, v. 6, no. 5, p. 309–314, doi:10.2113/gselements.6.5.309.

Powell, R and Holland, TJB 2008, On thermobarometry: Journal of Metamorphic Geology, v. 26, no. 2, p. 155–179.

Thermometers and barometers

Ferry, JM and Watson, EB 2007, New thermodynamic models and revised calibrations for the Ti-in-zircon and Zr-in-rutile thermometers: Contributions to Mineralogy and Petrology, v. 154, no. 4, p. 429–437, doi:10.1007/s00410-007-0201-0.

Hayden, LA, Watson, EB and Wark, DA 2008, A thermobarometer for sphene (titanite): Contributions to Mineralogy and Petrology, v. 155, no. 4, p. 529–540, doi:10.1007/s00410-007-0256-y.

Kohn, MJ 2014, "Thermoba-Raman-try": Calibration of spectroscopic barometers and thermometers for mineral inclusions: Earth and Planetary Science Letters, v. 388, p. 187–196, 10p., doi:10.1016/j.epsl.2013.11.054.

Pyle, JM, Spear, FS, Rudnick, RL and McDonough, WF 2001, Monazite-xenotime-garnet equilibrium in metapelites and a new monazite-garnet thermometer: Journal of Petrology, v. 42, no. 11, p. 2083–2107.

Thomas, JB, Bruce Watson, E, Spear, FS, Shemella, PT, Nayak, SK and Lanzirotti, A 2010, TitaniQ under pressure: the effect of pressure and temperature on the solubility of Ti in quartz: Contributions to Mineralogy and Petrology, v. 160, no. 5, p. 743–759, doi:10.1007/s00410-010-0505-3.

Tomkins, HS, Powell, R and Ellis, DJ 2007, The pressure dependence of the zirconium-in-rutile thermometer: Journal of Metamorphic Geology, v. 25, no. 6, p. 703–713, doi:10.1111/j.1525-1314.2007.00724.x.

Wark, DA and Watson, EB 2006, TitaniQ: a titanium-in-quartz geothermometer: Contributions to Mineralogy and Petrology, v. 152, no. 6, p. 743–754, doi:10.1007/s00410-006-0132-1.

Watson, EB, Wark, DA and Thomas, JB 2006, Crystallization thermometers for zircon and rutile: Contributions to Mineralogy and Petrology, v. 151, no. 4, p. 413–433, doi:10.1007/s00410-006-0068-5.

Zack, T, Moraes, R and Kronz, A 2004, Temperature dependence of Zr in rutile: empirical calibration of a rutile thermometer: Contributions to Mineralogy and Petrology, v. 148, no. 4, p. 471–488, doi:10.1007/s00410-004-0617-8.

Phase equilibria modelling — some recent examples

Prograde metamorphism

Guiraud, M, Powell, R and Rebay, G 2001, H_2O in metamorphism and unexpected behaviour in the preservation of metamorphic mineral assemblages: Journal of Metamorphic Geology, v. 19, no. 4, p. 445–454.

Yakymchuk, C and Brown, M 2014, Consequences of open-system melting in tectonics: Journal of the Geological Society, v. 171, no. 1, p. 21–40, doi:10.1144/jgs2013-039.

Retrograde metamorphism

Brown, M 2002, Retrograde processes in migmatites and granulites revisited: Journal of Metamorphic Geology, v. 20, p. 25–40.

Kelsey, DE, Morrissey, LJ, Hand, M, Clark, C, Tamblyn, R, Gaehl, AA and Marshall, S 2017, Significance of post-peak metamorphic reaction microstructures in the ultrahigh temperature Eastern Ghats Province, India: Journal of Metamorphic Geology, v. 35, no. 9, p. 1081–1109, doi:10.1111/jmg.12277.

White, RW and Powell, R 2011, On the interpretation of retrograde reaction textures in granulite facies rocks: Journal of Metamorphic Geology, v. 29, no. 1, p. 131–149, doi:10.1111/j.1525-1314.2010.00905.x.

Partial melting and melt loss

Korhonen, FJ, Saito, S, Brown, M and Siddoway, CS 2010, Modeling multiple melt loss events in the evolution of an active continental margin: Lithos, v. 116, 3-4, p. 230–248, doi:10.1016/j.lithos.2009.09.004.

Palin, RM, White, RW, Green, ECR, Diener, JFA, Powell, R and Holland, TJB 2016, High-grade metamorphism and partial melting of basic and intermediate rocks: Journal of Metamorphic Geology, v. 34, no. 9, p. 871–892, doi:10.1111/jmg.12212.

Palin, RM, White, RW and Green, ECR 2016, Partial melting of metabasic rocks and the generation of tonalitic–trondhjemitic–granodioritic (TTG) crust in the Archaean: Constraints from phase equilibrium modelling: Precambrian Research, v. 287, p. 73–90, doi:10.1016/j.precamres.2016.11.001.

White, R and Powell, R 2002, Melt loss and preservation of granulite facies mineral assemblages: Journal of Metamorphic Geology, v. 20, p. 621–632.

White, RW, Palin, RM and Green, ECR 2017, High-grade metamorphism and partial melting in Archean composite grey gneiss complexes: Journal of Metamorphic Geology, v. 35, no. 2, p. 181–195, doi:10.1111/jmg.12227.

White, RW, Powell, R and Halpin, JA 2004, Spatially-focussed melt formation in aluminous metapelites from Broken Hill, Australia: Journal of Metamorphic Geology, v. 22, no. 9, p. 825–845.

White, RW, Powell, R and Holland, TJB 2001, Calculation of partial melting equilibria in the system Na_2O–CaO–K_2O–FeO–MgO–Al_2O_3–SiO_2–H_2O (NCKFMASH): Journal of Metamorphic Geology, v. 19, no. 2, p. 139–153.

Melt addition

Bartoli, O 2017, Phase equilibria modelling of residual migmatites and granulites: An evaluation of the melt-reintegration approach: Journal of Metamorphic Geology, v. 35, no. 8, p. 919–942, doi:10.1111/jmg.12261.

Korhonen, FJ, Brown, M, Clark, C and Bhattacharya, S 2013, Osumilite-melt interactions in ultrahigh temperature granulites: phase equilibria modelling and implications for the P-T-t evolution of the Eastern Ghats Province, India: Journal of Metamorphic Geology, v. 31, no. 8, p. 881–907.

Role of water

Carson, CJ, Powell, R and Clarke, GL 1999, Calculated mineral equilibria for eclogites in CaO–Na_2O–FeO–MgO–Al_2O_3–SiO_2–H_2O: application to the Pouébo Terrane, Pam Peninsula, New Caledonia: Journal of Metamorphic Geology, v. 17, no. 1, p. 9–24, 16p.

Guiraud, M, Powell, R and Rebay, G 2001, H_2O in metamorphism and unexpected behaviour in the preservation of metamorphic mineral assemblages: Journal of Metamorphic Geology, v. 19, no. 4, p. 445–454.

Webb, G, Powell, R and McLaren, S 2015, Phase equilibria constraints on the melt fertility of crustal rocks: the effect of subsolidus water loss: Journal of Metamorphic Geology, v. 33, no. 2, p. 147–165, doi:10.1111/jmg.12114.

Metasomatism and alteration

Corriveau, L, Blein, O, Gervais, F, Trapy, PH, Souza, S de and Fafard, D 2018, Iron-oxide and alkali-calcic alteration, skarn, and epithermal mineralizing systems of the Grenville Province: the Bondy gneiss complex in the Central Metasedimentary Belt of Quebec as a case example — a field trip to the 14th Society for Geology Applied to Mineral Deposits (SGA) biennial meeting: Geological Survey of Canada; Open File 8349, 125p., doi:10.4095/311230.

Corriveau, L, Montreuil, J-F and Potter, EG 2016, Alteration Facies Linkages Among Iron Oxide Copper-Gold, Iron Oxide-Apatite, and Affliated Deposits in the Great Bear Magmatic Zone, Northwest Territories, Canada: Economic Geology, v. 111, p. 2045–2072.

Elmer, FL, Powell, R, White, RW and Phillips, GN 2007, Timing of Gold Mineralization Relative to the Peak of Metamorphism at Bronzewing, Western Australia: Economic Geology, v. 102, p. 379–392.

Elmer, FL, White, RW and Powell, R 2006, Devolatilization of metabasic rocks during greenschist-amphibolite facies metamorphism: Journal of Metamorphic Geology, v. 24, no. 6, p. 497–513, doi:10.1111/j.1525-1314.2006.00650.x.

Evans, KA 2010, A test of the viability of fluid–wall rock interaction mechanisms for changes in opaque phase assemblage in metasedimentary rocks in the Kambalda-St. Ives goldfield, Western Australia: Mineralium Deposita, v. 45, no. 2, p. 207–213, doi:10.1007/s00126-009-0260-4.

Evans, KA, Powell, R and Frost, BR 2013, Using equilibrium thermodynamics in the study of metasomatic alteration, illustrated by an application to serpentinites: Lithos, v. 168–169, p. 67–84, doi:10.1016/j.lithos.2013.01.016.

White, RW, Powell, R and Phillips, GN 2003, A mineral equilibria study of the hydrothermal alteration in mafic greenschist facies rocks at Kalgoorlie, Western Australia: Journal of Metamorphic Geology, v. 21, p. 455–468.

Mantle melting

Holland, TJB, Green, ECR and Powell, R 2018, Melting of Peridotites through to Granites: A Simple Thermodynamic Model in the System KNCFMASHTOCr: Journal of Petrology, v. 59, no. 5, p. 881–900, doi:10.1093/petrology/egy048.

Holland, TJB, Hudson, NFC, Powell, R and Harte, B 2013, New Thermodynamic Models and Calculated Phase Equilibria in NCFMAS for Basic and Ultrabasic Compositions through the Transition Zone into the Uppermost Lower Mantle: Journal of Petrology, v. 54, no. 9, p. 1901–1920, doi:10.1093/petrology/egt035.

Jennings, ES and Holland, TJB 2015, A Simple Thermodynamic Model for Melting of Peridotite in the System NCFMASOCr: Journal of Petrology, v. 56, no. 5, p. 869–892, doi:10.1093/petrology/egv020.

Mineralization

Tomkins, AG 2010, Windows of metamorphic sulfur liberation in the crust: Implications for gold deposit genesis: Geochimica et Cosmochimica Acta, v. 74, no. 11, p. 3246–3259.

Tomkins, AG and Grundy, C 2009, Upper temperature limits of orogenic gold deposit formation: Constraints from the granulite-hosted Griffin's Find deposit, Yilgarn Craton: Economic Geology, v. 104, no. 5, p. 669–685.

Zhong, R, Brugger, J, Chen, Y and Li, W 2015, Contrasting regimes of Cu, Zn and Pb transport in ore-forming hydrothermal fluids: Chemical Geology, v. 395, p. 154–164, doi:10.1016/j.chemgeo.2014.12.008.

Zhong, R, Brugger, J, Tomkins, AG, Chen, Y and Li, W 2015, Fate of gold and base metals during metamorphic devolatilization of a pelite: Geochimica et Cosmochimica Acta, v. 171, p. 338–352, doi:10.1016/j.gca.2015.09.013.

Phase equilibria behaviour of accessory phases

Kelsey, DE, Clark, C and Hand, M 2008, Thermobarometric modelling of zircon and monazite growth in melt-bearing systems: Examples using model metapelitic and metapsammitic granulites: Journal of Metamorphic Geology, v. 26, p. 199–212.

Kelsey, DE and Powell, R 2011, Progress in linking accessory mineral growth and breakdown to major mineral evolution in metamorphic rocks: a thermodynamic approach in the Na_2O–CaO–K_2O–FeO–MgO–Al_2O_3–SiO_2–H_2O–TiO_2–ZrO_2 system: Journal of Metamorphic Geology, v. 29, no. 1, p. 151–166, doi:10.1111/j.1525-1314.2010.00910.x.

Spear, FS 2010, Monazite-allanite phase relations in metapelites: Chemical Geology, v. 279, no. 1, p. 55–62.

Spear, FS and Pyle, JM 2010, Theoretical modeling of monazite growth in a low-Ca metapelite: Chemical Geology, v. 273, 1-2, p. 111–119, doi:10.1016/j.chemgeo.2010.02.016.

Yakymchuk, C 2017, Behaviour of apatite during partial melting of metapelites and consequences for prograde suprasolidus monazite growth: Lithos, v. 274–275, p. 412–426, doi:10.1016/j.lithos.2017.01.009.

Yakymchuk, C and Brown, M 2014, Behaviour of zircon and monazite during crustal melting: Journal of the Geological Society, v. 171, no. 4, p. 465–479, doi:10.1144/jgs2013-115.

Geodynamic and geochemical (re)cycling models

Evans, KA and Powell, R 2015, The effect of subduction on the sulphur, carbon and redox budget of lithospheric mantle: Journal of Metamorphic Geology, v. 33, no. 6, p. 649–670, doi:10.1111/jmg.12140.

Johnson, TE, Brown, M, Kaus, BJ and Vantongeren, JA 2013, Delamination and recycling of Archaean crust caused by gravitational instabilities: Nature Geoscience, v. 7, no. 1, p. 47–52, doi:10.1038/ngeo2019.

Kerrick, DM and Connolly, JAD 2001, Metamorphic devolatilization of subducted oceanic metabasalts: implications for seismicity, arc magmatism and volatile recycling: Earth and Planetary Science Letters, v. 189, p. 19–29.

Palin, RM and White, RW 2015, Emergence of blueschists on Earth linked to secular changes in oceanic crust composition: Nature Geoscience, v. 9, no. 1, p. 60–64, doi:10.1038/ngeo2605.

Chemical systems and rock types

Evans, KA, Powell, R and Holland, TJB 2010, Internally consistent data for sulphur-bearing phases and application to the construction of pseudosections for mafic greenschist facies rocks in Na_2O–CaO–K_2O–FeO–MgO–Al_2O_3–SiO_2–CO_2–O–S–H_2O: Journal of Metamorphic Geology, v. 28, no. 6, p. 667–687, doi:10.1111/j.1525-1314.2010.00890.x.

Green, ECR, White, RW, Diener, JFA, Powell, R, Holland, TJB and Palin, RM 2016, Activity-composition relations for the calculation of partial melting equilibria in metabasic rocks: Journal of Metamorphic Geology, v. 34, no. 9, p. 845–869.

Holland, TJB, Green, ECR and Powell, R 2018, Melting of Peridotites through to Granites: A Simple Thermodynamic Model in the System KNCFMASHTOCr: Journal of Petrology, v. 59, no. 5, p. 881–900, doi:10.1093/petrology/egy048.

Holland, TJB, Hudson, NFC, Powell, R and Harte, B 2013, New Thermodynamic Models and Calculated Phase Equilibria in NCFMAS for Basic and Ultrabasic Compositions through the Transition Zone into the Uppermost Lower Mantle: Journal of Petrology, v. 54, no. 9, p. 1901–1920, doi:10.1093/petrology/egt035.

Jennings, ES and Holland, TJB 2015, A Simple Thermodynamic Model for Melting of Peridotite in the System NCFMASOCr: Journal of Petrology, v. 56, no. 5, p. 869–892, doi:10.1093/petrology/egv020.

White, RW, Powell, R, Holland, TJB, Johnson, TE and Green, ECR 2014, New mineral activity-composition relations for thermodynamic calculations in metapelitic systems: Journal of Metamorphic Geology, v. 32, no. 3, p. 261–286.

White, RW, Powell, R, Holland, TJB and Worley, BA 2000, The effect of TiO_2 and Fe_2O_3 on metapelitic assemblages at greenschist and amphibolite facies conditions: Mineral equilibria calculations in the system K_2O–FeO–MgO–Al_2O_3–SiO_2–H_2O–TiO_2–Fe_2O_3: Journal of Metamorphic Geology, v. 18, no. 5, p. 497–511.

White, RW, Powell, R and Johnson, TE 2014, The effect of Mn on mineral stability in metapelites revisited: New a-x relations for manganese-bearing minerals: Journal of Metamorphic Geology, v. 32, no. 8, p. 809–828, doi:10.1111/jmg.12095.

Effect of Mn on garnet stability

Mahar, EM, Baker, JM, Powell, R, Holland, TJB and Howell, N 1997, The effect of Mn on mineral stability in metapelites: Journal of Metamorphic Geology, v. 15, no. 2, p. 223–238.

Tinkham, DK, Zuluaga, CA and Stowell, HH 2001, Metapelitic phase equilibria modelling in MnNCKFMASH: The effect of variable Al_2O_3 and MgO/(MgO + FeO) on mineral stability: Geological Materials Research, v. 3, p. 1–42.

White, RW, Powell, R and Johnson, TE 2014, The effect of Mn on mineral stability in metapelites revisited: New a-x relations for manganese-bearing minerals: Journal of Metamorphic Geology, v. 32, no. 8, p. 809–828, doi:10.1111/jmg.12095.

Bulk composition

Evans, TP 2004, A method for calculating effective bulk composition modification due to crystal fractionation in garnet-bearing schist: implications for isopleth thermobarometry: Journal of Metamorphic Geology, v. 22, no. 6, p. 547–557, doi:10.1111/j.1525-1314.2004.00532.x.

Guevara, VE and Caddick, MJ 2016, Shooting at a moving target: phase equilibria modelling of high-temperature metamorphism: Journal of Metamorphic Geology, v. 34, no. 3, p. 209–235, doi:10.1111/jmg.12179.

Palin, RM, Weller, OM, Waters, DJ and Dyck, B 2016, Quantifying geological uncertainty in metamorphic phase equilibria modelling; a Monte Carlo assessment and implications for tectonic interpretations: Geoscience Frontiers, v. 7, no. 4, p. 591–607, doi:10.1016/j.gsf.2015.08.005.

Powell, R and Holland, TJB 2008, On thermobarometry: Journal of Metamorphic Geology, v. 26, no. 2, p. 155–179.

Stüwe, K 1997, Effective bulk composition changes due to cooling: a model predicting complexities in retrograde reaction textures: Contributions to Mineralogy and Petrology, v. 129, p. 43–52.

Domainal bulk composition

Stüwe, K 1997, Effective bulk composition changes due to cooling: a model predicting complexities in retrograde reaction textures: Contributions to Mineralogy and Petrology, v. 129, p. 43–52.

White, RW and Powell, R 2011, On the interpretation of retrograde reaction textures in granulite facies rocks: Journal of Metamorphic Geology, v. 29, no. 1, p. 131–149, doi:10.1111/j.1525-1314.2010.00905.x.

White, RW, Powell, R and Baldwin, JA 2008, Calculated phase equilibria involving chemical potentials to investigate the textural evolution of metamorphic rocks: Journal of Metamorphic Geology, v. 26, no. 2, p. 181–198, doi:10.1111/j.1525-1314.2008.00764.x.

Zibra, I, Korhonen, FJ, Peternell, M, Weinberg, RF, Romano, SS, Braga, R, de Paoli, MC and Roberts, M 2017, On thrusting, regional unconformities and exhumation of high-grade greenstones in Neoarchean orogens: the case of the Waroonga Shear Zone, Yilgarn Craton: Tectonophysics, v. 712–713, p. 362–395, doi:10.1016/j.tecto.2017.05.017.

Diffusion and cation transport

Carlson, WD 2002, Scales of disequilibrium and rates of equilibration during metamorphism: American Mineralogist, v. 87, p. 185–204, 20p.

Carlson, WD 2012, Rates and mechanism of Y, REE, and Cr diffusion in garnet: American Mineralogist, v. 97, no. 10, p. 1598–1618, doi:10.2138/am.2012.4108.

Carlson, WD, Pattison, DRM and Caddick, MJ 2015, Beyond the equilibrium paradigm: How consideration of kinetics enhances metamorphic interpretation: American Mineralogist, v. 100, no. 8–9, p. 1659–1667, doi:10.2138/am-2015-5097.

Ganguly, J 2002, Diffusion kinetics in minerals: principles and applications to tectono-metamorphic processes: EMU Notes in Mineralogy, v. 4, p. 271–309.

Effects of H_2O on mineral equilibria

Carson, CJ, Powell, R and Clarke, GL 1999, Calculated mineral equilibria for eclogites in $CaO–Na_2O–FeO–MgO–Al_2O_3–SiO_2–H_2O$: application to the Pouébo Terrane, Pam Peninsula, New Caledonia: Journal of Metamorphic Geology, v. 17, no. 1, p. 9–24.

Guiraud, M, Powell, R and Rebay, G 2001, H_2O in metamorphism and unexpected behaviour in the preservation of metamorphic mineral assemblages: Journal of Metamorphic Geology, v. 19, no. 4, p. 445–454.

Kelsey, DE and Hand, M 2015, On ultrahigh temperature crustal metamorphism: Phase equilibria, trace element thermometry, bulk composition, heat sources, timescales and tectonic settings: Geoscience Frontiers, v. 6, no. 3, p. 311–356, doi:10.1016/j.gsf.2014.09.006.

Korhonen, FJ, Powell, R and Stout, JH 2012, Stability of sapphirine + quartz in the oxidized rocks of the Wilson Lake terrane, Labrador: Calculated equilibria in NCKFMASHTO: Journal of Metamorphic Geology, v. 30, no. 1, p. 21–36.

Powell, R and Downes, J 1990, Chapter 5 Garnet porphyroblast-bearing leucosomes in metapelites: mechanisms, phase diagrams, and an example from Broken Hill, Australia, *in* High-temperature Metamorphism and Crustal Anatexis *edited by* JR Ashworth and M Brown: The Mineral Society Series, Kluwer Academic Publishers, London, UK, p. 105–123.

Webb, G, Powell, R and McLaren, S 2015, Phase equilibria constraints on the melt fertility of crustal rocks: the effect of subsolidus water loss: Journal of Metamorphic Geology, v. 33, no. 2, p. 147–165, doi:10.1111/jmg.12114.

White, R and Powell, R 2002, Melt loss and preservation of granulite facies mineral assemblages: Journal of Metamorphic Geology, v. 20, p. 621–632.

White, RW and Powell, R 2010, Retrograde melt-residue interaction and the formation of near-anhydrous leucosomes in migmatites: Journal of Metamorphic Geology, v. 28, no. 6, p. 579–597, doi:10.1111/j.1525-1314.2010.00881.x.

White, RW, Powell, R and Holland, TJB 2001, Calculation of partial melting equilibria in the system $Na_2O–CaO–K_2O–FeO–MgO–Al_2O_3–SiO_2–H_2O$ (NCKFMASH): Journal of Metamorphic Geology, v. 19, no. 2, p. 139–153.

Effects of Fe_2O_3 on mineral equilibria

Boger, SD, White, RW and Schulte, B 2012, The importance of iron speciation (Fe^{+2}/Fe^{+3}) in determining mineral assemblages: an example from the high-grade aluminous metapelites of southeastern Madagascar: Journal of Metamorphic Geology, v. 30, no. 9, p. 997–1018, doi:10.1111/jmg.12001.

Korhonen, FJ, Powell, R and Stout, JH 2012, Stability of sapphirine + quartz in the oxidized rocks of the Wilson Lake terrane, Labrador: Calculated equilibria in NCKFMASHTO: Journal of Metamorphic Geology, v. 30, no. 1, p. 21–36.

White, RW, Powell, R and Clarke, GL 2002, The interpretation of reaction textures in Fe-rich metapelitic granulites of the Musgrave Block, central Australia: Constraints from mineral equilibria calculations in the system $K_2O–FeO–MgO–Al_2O_3–SiO_2–H_2O–TiO_2–Fe_2O_3$: Journal of Metamorphic Geology, v. 20, no. 1, p. 41–55.

White, RW, Powell, R, Holland, TJB and Worley, BA 2000, The effect of TiO_2 and Fe_2O_3 on metapelitic assemblages at greenschist and amphibolite facies conditions: Mineral equilibria calculations in the system $K_2O–FeO–MgO–Al_2O_3–SiO_2–H_2O–TiO_2–Fe_2O_3$: Journal of Metamorphic Geology, v. 18, no. 5, p. 497–511.

Fe titration

Fitton, JG and Gill, RCO 1970, The oxidation of ferrous iron in rocks during mechanical grinding: Geochimica et Cosmochimica Acta, v. 34, no. 4, p. 518–524.

Saikkonen, RJ and Rautiainen, IA 1993, Determination of ferrous iron in rock and mineral samples by three volumetric methods: Bulletin of the Geological Society of Finland, v. 65, no. 1, p. 59–63.

Fe^{3+} estimation by stoichiometry

Droop, GTR 1987, A general equation for estimating Fe^{3+} concentrations in ferromagnesian silicates and oxides from microprobe analyses, using stoichiometric criteria: Mineralogical Magazine, v. 51, no. 361, p. 431–435.

Schumacher, JC 1991, Empirical ferric iron corrections: necessity, assumptions, and effects on selected geothermobarometers: Mineralogical Magazine, v. 55, no. 378, p. 3–18.

P–T–t path and interpretation

England, PC and Thompson, AB 1984, Pressure-temperature-time paths of regional metamorphism I. Heat transfer during the evolution of thickened continental crust: Journal of Petrology, v. 25, no. 4, p. 894–928.

Kelsey, DE and Hand, M 2015, On ultrahigh temperature crustal metamorphism: Phase equilibria, trace element thermometry, bulk composition, heat sources, timescales and tectonic settings: Geoscience Frontiers, v. 6, no. 3, p. 311–356, doi:10.1016/j.gsf.2014.09.006.

Sizova, E, Gerya, T and Brown, M 2014, Contrasting styles of Phanerozoic and Precambrian continental collision: Gondwana Research, v. 25, no. 2, p. 522–545, doi:10.1016/j.gr.2012.12.011.

Sizova, E, Gerya, T, Brown, M and Stüwe, K 2018, What drives metamorphism in early Archean greenstone belts? Insights from numerical modeling: Tectonophysics, v. 746, p. 587–601, doi:10.1016/j.tecto.2017.07.020.

Spear, FS 1993, Metamorphic phase equilibria and pressure-temperature-time paths: Mineralogical Society of America, Monograph, 799p.

Thompson, AB and England, PC 1984, Pressure-temperature-time paths of regional metamorphism II: their inference and interpretation using mineral assemblages in metamorphic rocks: Journal of Petrology, v. 25, no. 4, p. 929–955.

Clockwise trajectories

England, PC and Richardson, SH 1977, The influence of erosion upon the mineral facies of rocks from different metamorphic environments: Journal of the Geological Society, v. 134, p. 201–213.

England, PC and Thompson, AB 1984, Pressure-temperature-time paths of regional metamorphism I. Heat transfer during the evolution of thickened continental crust: Journal of Petrology, v. 25, no. 4, p. 894–928.

Anticlockwise trajectories

Harley, SL 1989, The origins of granulites: a metamorphic perspective, v. 126, no. 3, p. 215–247.

Sandiford, M and Powell, R 1986, Deep crustal metamorphism during continental extension: modern and ancient examples: Earth and Planetary Science Letters, v. 79, no. 1–2, p. 151–158.

Constraining the *P–T* path

Relationship between inclusion and host

Vernon, RH, White, RW and Clarke, GL 2008, False metamorphic events inferred from misinterpretation of microstructural evidence and P–T data: Journal of Metamorphic Geology, v. 26, no. 4, p. 437–449.

Mineral zoning

Bhowany, K, Hand, M, Clark, C, Kelsey, DE, Reddy, SM, Pearce, MA, Tucker, NM and Morrissey, LJ 2018, Phase equilibria modelling constraints on P-T conditions during fluid catalysed conversion of granulite to eclogite in the Bergen Arcs, Norway: Journal of Metamorphic Geology, v. 36, no. 3, p. 315–342, doi:10.1111/jmg.12294.

Caddick, MJ, Konopásek, J and Thompson, AB 2010, Preservation of Garnet Growth Zoning and the Duration of Prograde Metamorphism: Journal of Petrology, v. 51, no. 11, p. 2327–2347, doi:10.1093/petrology/egq059.

Cutts, KA, Hand, M, Kelsey, DE and Strachan, RA 2009, Orogenic versus extensional settings for regional metamorphism: Knoydartian events in the Moine Supergroup revisited: Journal of the Geological Society, v. 166, no. 2, p. 201–204, doi:10.1144/0016-76492008-015.

Konrad-Schmolke, M, O'Brien, PJ, Capitani, C de and Carswell, DA 2008, Garnet growth at high- and ultra-high pressure conditions and the effect of element fractionation on mineral modes and composition: Lithos, v. 103, no. 3–4, p. 309–332, doi:10.1016/j.lithos.2007.10.007.

Konrad-Schmolke, M, Zack, T, O'Brien, PJ and Jacob, DE 2008, Combined thermodynamic and rare earth element modelling of garnet growth during subduction: Examples from ultrahigh-pressure eclogite of the Western Gneiss Region, Norway: Earth and Planetary Science Letters, v. 272, no. 1–2, p. 488–498, doi:10.1016/j.epsl.2008.05.018.

Spear, FS and Selverstone, J 1983, Quantitative PT paths from zoned minerals: Theory and tectonic applications: Contributions to Mineralogy and Petrology, v. 83, no. 3–4, p. 348–357.

Spear, FS, Selverstone, J, Hickmott, D, Crowley, P and Hodges, KV 1984, P-T paths from garnet zoning: A new technique for deciphering tectonic processes in crystalline terranes: Geology, v. 12, p. 87–90.

Vance, D, Strachan, RA and Jones, KA 1998, Extensional versus compressional settings for metamorphism: garnet chronometry and pressure-temperature-time histories in the Moine Supergroup, northwest Scotland: Geology, v. 26, no. 10, p. 927–930.

Homogenized zoning

Fitzsimons, ICW and Harley, SL 1994, The Influence of Retrograde Cation Exchange on Granulite P-T Estimates and a Convergence Technique for the Recovery of Peak Metamorphic Conditions: Journal of Petrology, v. 35, no. 2, p. 543–576.

Florence, FP and Spear, FS 1991, Effects of diffusional modification of garnet growth zoning on P-T path calculations: Contributions to Mineralogy and Petrology, v. 107, p. 487–500.

Pattison, DRM and Bégin, NJ 1994, Zoning patterns in orthopyroxene and garnet in granulites: implications for geothermometry: Journal of Metamorphic Geology, v. 12, p. 387–410.

Pattison, DRM, Chacko, T, Farquhar, J and McFarlane, CRM 2003, Temperatures of granulite-facies metamorphism: constraints from experimental phase equilibria and thermobarometry corrected for retrograde exchange: Journal of Petrology, v. 44, no. 5, p. 867–900.

Mineral reaction textures

Alessio, K, Hand, M, Morrissey, L, Kelsey, D and Payne, J 2017, Melt Reintegration Modelling: Testing against a Subsolidus Reference Assemblage: Geosciences, v. 7, no. 3, p. 75, doi:10.3390/geosciences7030075.

Ashworth, JR 1993, Fluid-absent diffusion kinetics of Al inferred from retrograde metamorphic coronas: American Mineralogist, v. 78, p. 331–337.

Ashworth, JR, Sheplev, VS, Bryxina, NA, Kolobov, VY, Reverdatto, VV 1998, Diffusion-controlled corona reaction and overstepping of equilibrium in a garnet granulite, Yenisey Ridge, Siberia: Journal of Metamorphic Geology, v. 16, p. 231–246.

Korhonen, FJ and Stout, JH 2005, Borosilicate- and phengite-bearing veins from the Grenville Province of Labrador: Evidence for rapid uplift: Journal of Metamorphic Geology, v. 23, no. 5, p. 297–311.

White, RW and Powell, R 2011, On the interpretation of retrograde reaction textures in granulite facies rocks: Journal of Metamorphic Geology, v. 29, no. 1, p. 131–149, doi:10.1111/j.1525-1314.2010.00905.x.

White, RW, Powell, R and Baldwin, JA 2008, Calculated phase equilibria involving chemical potentials to investigate the textural evolution of metamorphic rocks: Journal of Metamorphic Geology, v. 26, no. 2, p. 181–198, doi:10.1111/j.1525-1314.2008.00764.x.

Apparent thermal gradients and tectonic setting

Brown, M 2006, Duality of thermal regimes is the distinctive characteristic of plate tectonics since the Neoarchean: Geology, v. 34, no. 11, p. 961–964, doi:10.1130/G22853A.1.

Brown, M 2014, The contribution of metamorphic petrology to understanding lithosphere evolution and geodynamics: Geoscience Frontiers, v. 5, no. 4, p. 553–569.

Brown, M and Johnson, T 2018, Secular change in metamorphism and the onset of global plate tectonics: American Mineralogist, v. 103, no. 2, p. 181–196, doi:10.2138/am-2018-6166.

Spear, FS 1993, Metamorphic phase equilibria and pressure-temperature-time paths: Mineralogical Society of America, Monograph, 799p.

Stüwe, K 2007, Geodynamics of the lithosphere: An introduction: Springer, Berlin, 493p.

Uncertainties

Kinetic barriers for mineral equilibration and disequilibrium

Ague, JJ and Carlson, WD 2013, Metamorphism as Garnet Sees It: The Kinetics of Nucleation and Growth, Equilibration, and Diffusional Relaxation: Elements, v. 9, no. 6, p. 439–445, doi:10.2113/gselements.9.6.439.

Alessio, K, Hand, M, Morrissey, L, Kelsey, D and Payne, J 2017, Melt Reintegration Modelling: Testing against a Subsolidus Reference Assemblage: Geosciences, v. 7, no. 3, p. 75, doi:10.3390/geosciences7030075.

Carlson, WD, Pattison, DRM and Caddick, MJ 2015, Beyond the equilibrium paradigm: How consideration of kinetics enhances metamorphic interpretation: American Mineralogist, v. 100, 8-9, p. 1659–1667, doi:10.2138/am-2015-5097.

Gaidies, F, Pattison, DRM and Capitani, C de 2011, Toward a quantitative model of metamorphic nucleation and growth: Contributions to Mineralogy and Petrology, v. 162, no. 5, p. 975–993, doi:10.1007/s00410-011-0635-2.

Pattison, DRM, Capitani, C de and Gadies, F 2011, Petrological consequences of variations in metamorphic reaction affinity: Journal of Metamorphic Geology, v. 29, no. 9, p. 953–977, doi:10.1111/j.1525-1314.2011.00950.x.

Pattison, DRM and Spear, FS 2018, Kinetic control of staurolite-Al_2SiO_5 mineral assemblages: Implications for Barrovian and Buchan metamorphism: Journal of Metamorphic Geology, v. 36, no. 6, p. 667–690, doi:10.1111/jmg.12302.

Ridley, J and Thompson, AB 1986, The role of mineral kinetics in the development of metamorphic microtexture, *in* Fluid-Rock Interactions During Metamorphism *edited by* JV Walther and BJ Wood: Advances in Physical Geochemistry, v. 5, Springer, New York, p. 154–193.

Spear, FS and Pattison, DRM 2017, The implications of overstepping for metamorphic assemblage diagrams (MADs): Chemical Geology, v. 457, p. 38–46, doi:10.1016/j.chemgeo.2017.03.011.

Changes to bulk composition during metamorphism

Alessio, K, Hand, M, Morrissey, L, Kelsey, D and Payne, J 2017, Melt Reintegration Modelling: Testing against a Subsolidus Reference Assemblage: Geosciences, v. 7, no. 3, p. 75, doi:10.3390/geosciences7030075.

Bartoli, O 2017, Phase equilibria modelling of residual migmatites and granulites: An evaluation of the melt-reintegration approach: Journal of Metamorphic Geology, v. 35, no. 8, p. 919–942, doi:10.1111/jmg.12261.

Brown, M 2002, Retrograde processes in migmatites and granulites revisited: Journal of Metamorphic Geology, v. 20, p. 25–40.

Brown, M and Korhonen, FJ 2009, Some remarks on melting and extreme metamorphism of crustal rocks, *in* Physics and chemistry of the Earth's interior *edited by* AK Gupta and S Dasgupta: Springer, New York, US, p. 67–87.

Gaidies, F, de Capitani, C and Abart, R 2008, THERIA_G: a software program to numerically model prograde garnet growth: Contributions to Mineralogy and Petrology, v. 155, no. 5, p. 657–671, doi:10.1007/s00410-007-0263-z.

Indares, A, White, RW and Powell, R 2008, Phase equilibria modelling of kyanite-bearing anatectic paragneisses from the central Grenville Province: Journal of Metamorphic Geology, v. 26, no. 8, p. 815–836.

Korhonen, FJ, Brown, M, Clark, C and Bhattacharya, S 2013, Osumilite-melt interactions in ultrahigh temperature granulites: phase equilibria modelling and implications for the P-T-t evolution of the Eastern Ghats Province, India: Journal of Metamorphic Geology, v. 31, no. 8, p. 881–907.

Marmo, BA, Clarke, GL and Powell, R 2002, Fractionation of bulk rock composition due to porphyroblast growth: effects on eclogite facies mineral equilibria, Pam Peninsula, New Caledonia: Journal of Metamorphic Geology, v. 20, no. 1, p. 151–165.

Mayne, MJ, Stevens, G and Moyen, J-F 2019, A phase equilibrium investigation of selected source controls on the composition of melt batches generated by sequential melting of an average metapelite: Geological Society, London, Special Publications, v. 491, p. 223–241.

Moynihan, DP and Pattison, DRM 2013, An automated method for the calculation of P-T paths from garnet zoning, with application to metapelitic schist from the Kootenay Arc, British Columbia, Canada: Journal of Metamorphic Geology, v. 31, no. 5, p. 525–548, doi:10.1111/jmg.12032.

White, R and Powell, R 2002, Melt loss and preservation of granulite facies mineral assemblages: Journal of Metamorphic Geology, v. 20, p. 621–632.

White, RW, Powell, R and Halpin, JA 2004, Spatially-focussed melt formation in aluminous metapelites from Broken Hill, Australia: Journal of Metamorphic Geology, v. 22, no. 9, p. 825–845.

White, RW, Powell, R and Phillips, GN 2003, A mineral equilibria study of the hydrothermal alteration in mafic greenschist facies rocks at Kalgoorlie, Western Australia: Journal of Metamorphic Geology, v. 21, p. 455–468.

Yardley, BWD and Baltatzis, E 1985, Retrogression of staurolite schists and the sources of infiltrating fluids during metamorphism: Contributions to Mineralogy and Petrology, v. 89, p. 59–68.

Yardley, BWD and Bodnar, RJ 2014, Fluids in the continental crust: Geochemical Perspectives, v. 3, no. 1, p. 1–127, doi:10.7185/geochempersp.3.1.

Appendix 3

Abbreviations for common metamorphic minerals and phases

Abbreviation	*Mineral name*
Act	actinolite
Aeg	aegirine
Agt	aegirine–augite
Ab	albite
Afs	alkali feldspar
Aln	allanite
Alm	almandine
Als	aluminosilicate (Al_2SiO_5)
Amp	amphibole
And	andalusite
An	anorthite
Ath	anthophyllite
Ap	apatite
Aug	augite
Bdy	baddeleyite
Bt	biotite
Cal	calcite
Chl	chlorite
Cld	chloritoid
Cam	clinoamphibole
Cpx	clinopyroxene
Czo	clinozoisite
Coe	coesite
Crd	cordierite
Crn	corundum
Cum	cummingtonite
Di	diopside
Dol	dolomite
Ep	epidote
Fsp	feldspar
Fi	fibrolite (fibrous sillimanite)
Fo	forsterite
Grt	garnet
Ged	gedrite
Gln	glaucophane
Gr	graphite
Grs	grossular
Hem	hematite
Hc	hercynite
Hbl	hornblende
H_2O	fluid (water)
Ilm	ilmenite
Jd	jadeite
Kln	kaolinite
Kfs	K-feldspar
Ky	kyanite
Lws	lawsonite
Liq	liquid (silicate melt)
Mag	magnetite

Abbreviation	*Mineral name*
Mrg	margarite
Mca	mica
Mc	microcline
Mnz	monazite
Ms	muscovite
Omp	omphacite
Opq	opaque
Oam	orthoamphibole
Or	orthoclase
Opx	orthopyroxene
Osm	osumilite
Pg	paragonite
Ph	phengite
Phl	phlogopite
Pl	plagioclase
Prh	prehnite
Pmp	pumpellyite-(Al)
Py	pyrite
Prp	pyrope
Po	pyrrhotite
Px	pyroxene
Qz	quartz
Rt	rutile
Sa	sanadine
Spr	sapphirine
Scp	scapolite
Srl	schorl
Ser	sericite
Srp	serpentine
Sil	sillimanite
Sme	smectite
Sdl	sodalite
Sps	spessartine
Spl	spinel
Spd	spodumene
St	staurolite
Stp	stilpnomelane
Sti	stishovite
Str	strontianite
Tlc	talc
Thr	thorite
Ttn	titanite (sphene)
Tur	tourmaline
Tr	tremolite
Usp	ulvöspinel
Wo	wollanstonite
Xtm	xenotime
Zrn	zircon
Zo	zoisite

Note: Modified from Whitney and Evans (2010)

Reference

Whitney, DL and Evans, BW 2010, Abbreviations for Names of Rock-Forming Minerals: American Mineralogist, v. 95, p. 185–187.

RECORD 2020/14

This Record is published in digital format (PDF) and is available as a free download from the DMIRS website at <www.dmirs.wa.gov.au/GSWApublications>.

Further details of geoscience products are available from:

Information Centre
Department of Mines, Industry Regulation and Safety
100 Plain Street
EAST PERTH WESTERN AUSTRALIA 6004
Phone: +61 8 9222 3459 Email: publications@dmirs.wa.gov.au
www.dmirs.wa.gov.au/GSWApublications

THE UTILITY OF THE METAMORPHIC ROCK RECORD: CONSTRAINING THE PRESSURE–TEMPERATURE–TIME CONDITIONS OF METAMORPHISM

Korhonen et al.